Air Force Institute of Technology

AFIT Scholar

Theses and Dissertations | Student Graduate Works

3-2019

Infrared and Electro-Optical Stereo Vision for Automated Aerial Refueling

William E. Dallmann

Follow this and additional works at: https://scholar.afit.edu/etd

 Part of the Computer Engineering Commons, and the Optics Commons

Recommended Citation

Dallmann, William E., "Infrared and Electro-Optical Stereo Vision for Automated Aerial Refueling" (2019). *Theses and Dissertations*. 3588.
https://scholar.afit.edu/etd/3588

This Thesis is brought to you for free and open access by the Student Graduate Works at AFIT Scholar. It has been accepted for inclusion in Theses and Dissertations by an authorized administrator of AFIT Scholar. For more information, please contact richard.mansfield@afit.edu.

www.manaraa.com

INFRARED AND ELECTRO-OPTICAL STEREO VISION FOR AUTOMATED AERIAL REFUELING

THESIS

William E. Dallmann, Capt, USAF

AFIT-ENG-MS-19-M-022

DEPARTMENT OF THE AIR FORCE
AIR UNIVERSITY

AIR FORCE INSTITUTE OF TECHNOLOGY

Wright-Patterson Air Force Base, Ohio

DISTRIBUTION STATEMENT A
APPROVED FOR PUBLIC RELEASE; DISTRIBUTION UNLIMITED.

www.manaraa.com

The views expressed in this document are those of the author and do not reflect the official policy or position of the United States Air Force, the United States Department of Defense or the United States Government. This material is declared a work of the U.S. Government and is not subject to copyright protection in the United States.

www.manaraa.com

AFIT-ENG-MS-19-M-022

INFRARED AND ELECTRO-OPTICAL STEREO VISION FOR AUTOMATED AERIAL REFUELING

THESIS

Presented to the Faculty

Department of Electrical and Computer Engineering

Graduate School of Engineering and Management

Air Force Institute of Technology

Air University

Air Education and Training Command

in Partial Fulfillment of the Requirements for the

Degree of Master of Science in Computer Engineering

William E. Dallmann, B.S.E.E

Capt, USAF

March 2019

DISTRIBUTION STATEMENT A
APPROVED FOR PUBLIC RELEASE; DISTRIBUTION UNLIMITED.

www.manaraa.com

AFIT-ENG-MS-19-M-022

INFRARED AND ELECTRO-OPTICAL STEREO VISION FOR AUTOMATED AERIAL REFUELING

THESIS

William E. Dallmann, B.S.E.E
Capt, USAF

Committee Membership:

Dr. Scott L. Nykl
Chair

Dr. Douglas D. Hodson
Member

Dr. Robert C. Leishman
Member

Dr. Clark N. Taylor
Member

www.manaraa.com

Abstract

Currently, Unmanned Aerial Vehicles are unsafe to refuel in-flight due to the communication latency between the UAVs ground operator and the UAV. Providing UAVs with an in-flight refueling capability would improve their functionality by extending their flight duration and increasing their flight payload. Our solution to this problem is Automated Aerial Refueling (AAR) using stereo vision from stereo electro-optical and infrared cameras on a refueling tanker. To simulate a refueling scenario, we use ground vehicles to simulate a pseudo tanker and psuedo receiver UAV. Imagery of the receiver is collected by the cameras on the tanker and processed by a stereo block matching algorithm to calculate a position and orientation estimate of the receiver. GPS and IMU truth data is then used to validate these results.

www.manaraa.com

Acknowledgements

Thank you to my committee members for your involvement in my research. A special thank you to Dr. Nykl for my many questions he answered and for helping guide me through many challenges.

I would also like to thank my wife for the extra support she gave me while working on research. Her help made it possible for me to complete this research. Finally, I want to thank God for giving me this opportunity. All I have is from Him and He is my hope.

William E. Dallmann

www.manaraa.com

Table of Contents

www.manaraa.com

Page

www.manaraa.com

List of Figures

www.manaraa.com

www.manaraa.com

www.manaraa.com

List of Tables

www.manaraa.com

INFRARED AND ELECTRO-OPTICAL STEREO VISION FOR AUTOMATED AERIAL REFUELING

I. Introduction

Unmanned Aerial Vehicles (UAVs) are a relatively new technology that has seen a great increase in use over the past couple of decades. The United States Air Foce (USAF) relies on UAVs for accomplishing several types of missions, such as, surveillance or combat support. As technology improves, so do the capabilities of UAVs. For that reason, the use of UAVs will only continue to increase. UAVs do not have an on-board pilot, but are instead piloted by an operator at a remote location. UAVs, however, are set apart from manned aircraft by the fact that UAVs are not able to be refueled in-flight. Aerial refueling has a long history and is a regularly employed capability of the USAF. It is only reasonable that this technology should be extended to UAVs given their importance to the USAF.

In-flight refueling via the USAF's boom method requires precise movements from the receiver aircraft, which UAVs are incapable of performing. The limiting factor in the UAVs maneuverability is in the communication latency between the UAV and its remote operator. The operator is unable to make the required maneuvers as quickly as needed, which makes aerial refueling for UAVs dangerous. Providing the capability of aerial refueling to UAVs would have many benefits. Aerial refueling is often used to increase the flight duration of the aircraft being refueled and would certainly increase a UAVs flight duration. If the flight duration of the UAV can be increased, other possibilities are opened to the UAV, such as increasing the UAV's weapon payload. In-flight refueling would also reduce the cost associated with a UAV

www.manaraa.com

mission by eliminating the need to return to the ground for refueling.

The primary solution offered for solving this UAV problem is to make aerial refueling automated through a process called Automated Aerial Refueling (AAR). There have been multiple methods offered for accomplishing AAR, however, there is a fundamental problem that must be addressed to make AAR possible. The fundamental problem is that the relative position and orientation between the tanker and the receiver must be known. If this unknown can be solved, then the tanker can transmit a refueling flight path to the UAV with low latency, ultimately automating the refueling process. This research focuses on determining the position and orientation of the UAV from the tanker's perspective.

1.1 Problem Statement

The fundamental AAR problem boils down to answering the following question: how can the position and orientation of the UAV be determined? To answer that question, this research implements a stereo computer vision approach. In general, the stereo computer vision approach addresses the problem by reconstructing a 3D point cloud from a 2D image and finding the position and orientation estimates of the UAV from this point cloud. The first goal of this research was to validate electro-optical and infrared stereo vision systems for producing accurate estimates by recreating an aerial refueling scenario on the ground. The second goal was to validate the estimates using a highly accurate truth source, providing a way to make error assessments. The last goal was to create a framework for properly collecting stereo vision data for upcoming flight tests involving two C-12Cs acting as pseudo tanker and receiver.

www.manaraa.com

1.2 Assumptions

Certain assumptions had to be made to formulate reasonable experiments. Since ground experiments would take place on a flat surface, it was assumed that an aircraft being refueled would approach the tanker with a linear flight path. The linear flight path aids in equalizing the two situations because the receiver in the ground experiments is level with the ground plane. Next, it was assumed that the receiver would make contact with the tanker's refueling source at approximately 30 meters from the cameras. This assumption was made since the distance at contact point is an essential part of aerial refueling. Finally, it was assumed that the receiver aircraft would approach the tanker with the same look direction as the tanker. By assuming the look direction, a basic estimate can be made for the orientation of the receiver. This basic estimate serves as a starting point for computing the complete orientation estimate.

1.3 Contributions

The most impactful contribution of this research is the validation of IR stereo vision for pose estimation. IR stereo vision is a new method for finding pose estimation, and the results of this research show that IR stereo vision is highly accurate for pose estimation. Additionally, pose estimation using EO stereo vision is further validated in this research. Both the IR and EO results are consistent with each other, further showing that each system can compute an accurate pose estimate. The next contribution is the use of an Inertial Measurement Unit system combined with GPS to serve as the truth system for analyzing the results. This truth system provided a method for determining error in the pose estimates and for validating the results from both the IR and EO stereo vision systems. Finally, the experiments were completed in the real world and were modeled as closely as possible to a real refueling scenario.

www.manaraa.com

Therefore, these results are more applicable to AAR than results produced only from simulation.

1.4 Overview

This Thesis has five chapters, which are the Introduction, Background, Methodology, Results, and Conclusion. The current chapter, the Introduction, introduces the research problem. The Background chapter studies the previous work that has been completed in the AAR field. The Background also evaluates all of the techniques for creating pose estimates using stereo vision. The Methodology chapter provides an in-depth account of all of the processes and mechanisms used to setup experiments, collect data, and analyze the data. The Methodology outlines the ground experiments and how they were designed and completed. Additionally, the Methodology discusses virtual modeling of the experiments so they could be visualized and the results could be produced. The Results chapter lays out the pose estimation error from the experiments and discusses potential sources of error. Finally, the Conclusion chapter explores the impact of the results and provides improvements that can be made to the Methodology in future work.

www.manaraa.com

II. Background

2.1 Automated Aerial Refueling

The USAF is a world leader in air dominance and aircraft superiority. USAF aircraft are known for being some of the most capable and powerful aircraft known to the world. Although there are many technical and non-technical factors that contribute to the high performance of USAF aircraft, one of those factors is aerial refueling. Aerial refueling is the process of transferring fuel from one aircraft to another while in-flight. The aircraft supplying the fuel is defined as the tanker and the aircraft receiving the fuel is defined as the receiver.

There are two primary methods of aerial refueling within today's standards, the boom method and the probe-and-drogue method [5]. The probe-and-drogue method uses a long flexible pipe that transports fuel to a drogue at the end of the pipe. The receiver aircraft then has a probe that presses into the drogue to begin refueling. The boom method utilizes a rigid mechanical arm, called the boom, that extends out from the rear of the tanker. To refuel an aircraft, the boom connects to a refueling receptacle on the receiver and passes fuel from the tanker to the receiver through the boom. Currently, a boom operator aboard the tanker is the person responsible for mechanically operating the boom. The boom method is capable of refueling aircraft of various types, sizes, and shapes as seen in Figure 1 and Figure 2. The boom method will be the primary aerial refueling method considered in this research.

The boom method does have its challenges, however. The volume of space that an aircraft occupies while being refueled in-flight is called the refueling envelope. Therefore, the refueling envelope is not constant and depends on the size of the aircraft being refueled. Within the refueling envelope, the receiver must make precise movements to receive the boom and to maintain contact with the boom during refueling.

www.manaraa.com

Figure 1. Cargo Plane Aerial Refueling via Boom Method from USAF Tanker [1]

Figure 2. Nearby View of USAF Aircraft Aerial Refueling [2]

www.manaraa.com

Any aircraft that is incapable of performing the precise movements required for refueling would not be able to be refueled in-flight. This is the problem that (UAVs) face.

UAVs, by definition, do not have a pilot on-board. Instead, a UAV is controlled either autonomously or by a ground based operator. As outlined in [6], UAVs experience various forms of communication latency between the UAV and its operator. This communication latency prevents the UAV from making the precise movements required for aerial refueling. Therefore, Automated Aerial Refueling (AAR) is offered as a solution to the in-flight UAV refueling problem. AAR seeks to determine the position and orientation of the receiver, such that a flight path can be communicated directly from the tanker to the receiver. The receiver can then autonomously follow the communicated flight path in a precise manner to safely be refueled. For the purposes of this research, the position and orientation of an object collectively is defined as the object's pose.

Determining an aircraft's pose for AAR is accomplished through a means of pose estimation. If an inaccurate pose estimate is computed, the receiver would risk following an incorrect flight path, which would jeopardize the in-flight refueling. Therefore, the goal of pose estimation is to calculate the aircraft's pose as accurately as possible to the aircraft's true pose. This research focuses on using stereo vision as the method to accurately determine a receiver's pose. The use of stereo cameras for pose estimation is made possible through the equipping of stereo cameras on next-generation tankers, as indicated in [7].

2.2 Stereo Computer Vision

The key to pose estimation is through stereo vision is computer vision. Computer vision in its simplest terms is the modeling of imagery into a 3D environment using

www.manaraa.com

computer technology [8]. Computer vision seeks to model the environment in a manner similar to how human sight works. The human brain uses imagery from eyes and "computes" a 3D environment that is seen by the human. However, computer vision is challenged with determining many unknowns that makes modeling an environment to the accuracy of a human eye very difficult [8].

The image source is an important aspect of computer vision. Cameras, whether virtual or physical, are the most common source of imagery. Monocular vision is one form of vision which captures imagery using a single image source or camera. Likewise, stereo vision uses multiple image sources or cameras for capturing imagery. Therefore, stereo computer vision is the art of modeling a 3D environment using multiple sources of vision. For computer vision to be achievable, the stereo vision system itself must be modeled as described in Sections 2.3 - 2.5.

2.3 Pinhole Camera Model

Modeling the stereo vision system often begins with the pinhole camera model. At a basic level, an image is simply a set of pixels from the viewpoint of a computer. Therefore, much work must be done to take sets of pixels (images) and turn them into a 3D environment. The pinhole camera model translates properties of a camera into geometric and mathematical properties. These geometric and mathematical properties can then be used to determine unknowns about the pixels in the image. This translation of properties is shown in Figure 3.

The pinhole camera model is based on a tiny pinhole that defines how light passes through the aperature [9]. Referring to Figure 3, the camera's focal point F_c is centered in the pinhole camera model and defines the optical axis. The optical axis, Z_c, then passes through the center of a pinhole image plane at the principal point. Finally, refracted light from some point P in 3D space passes through a point (u, v)

www.manaraa.com

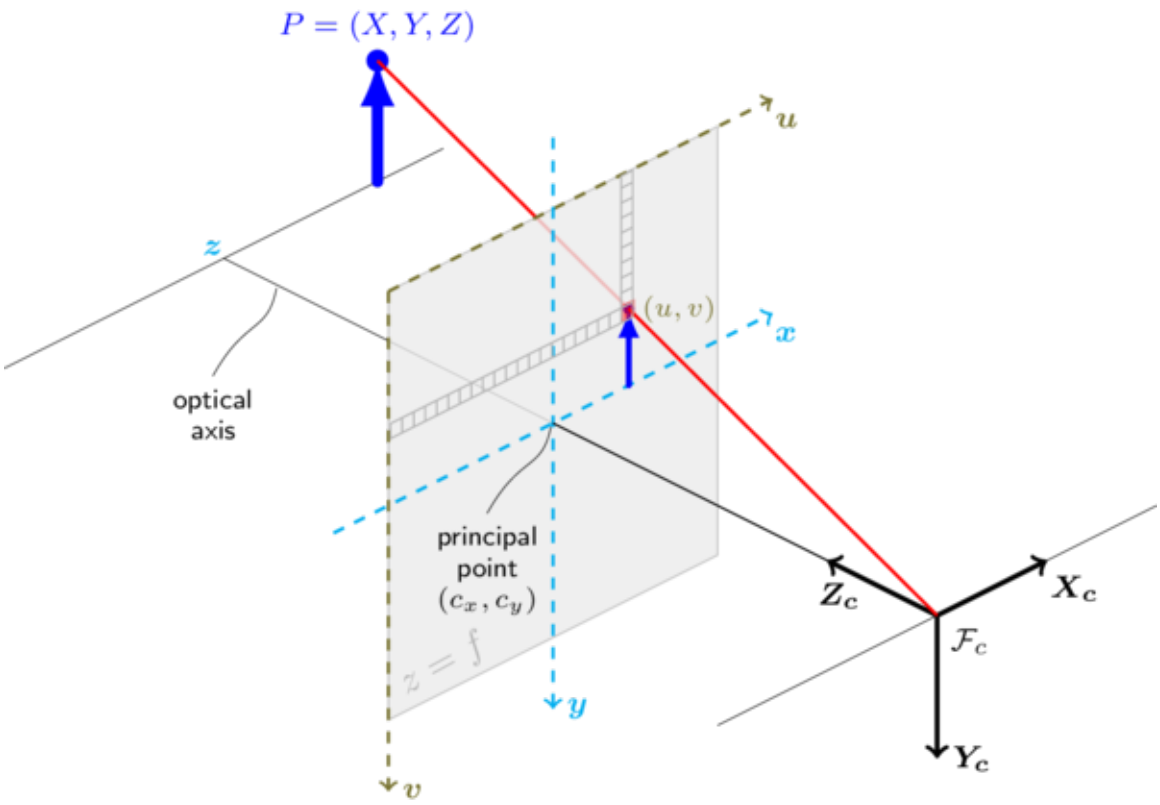

Figure 3. Pinhole Camera Model [3]

on the pinhole image plane. The point (u, v) on the image plane dictates the pixel in an image that shows point P. Ultimately, this geometric model helps extract a pixel's location in 3D space.

2.4 Epipolar Geometry

Since stereo vision makes use of multiple cameras, the geometric properties of each camera's pinhole model need to be modeled in the same system. This research utilizes a stereo vision system with two cameras, therefore, Epipolar Geometry can be used to relate the geometry of the first camera to the second camera. More specifically, Epipolar Geometry will relate the pixels of each camera that correspond to the same point in 3D space.

Given a point q in 3D space, an "epipolar" plane can be drawn amongst the points

www.manaraa.com

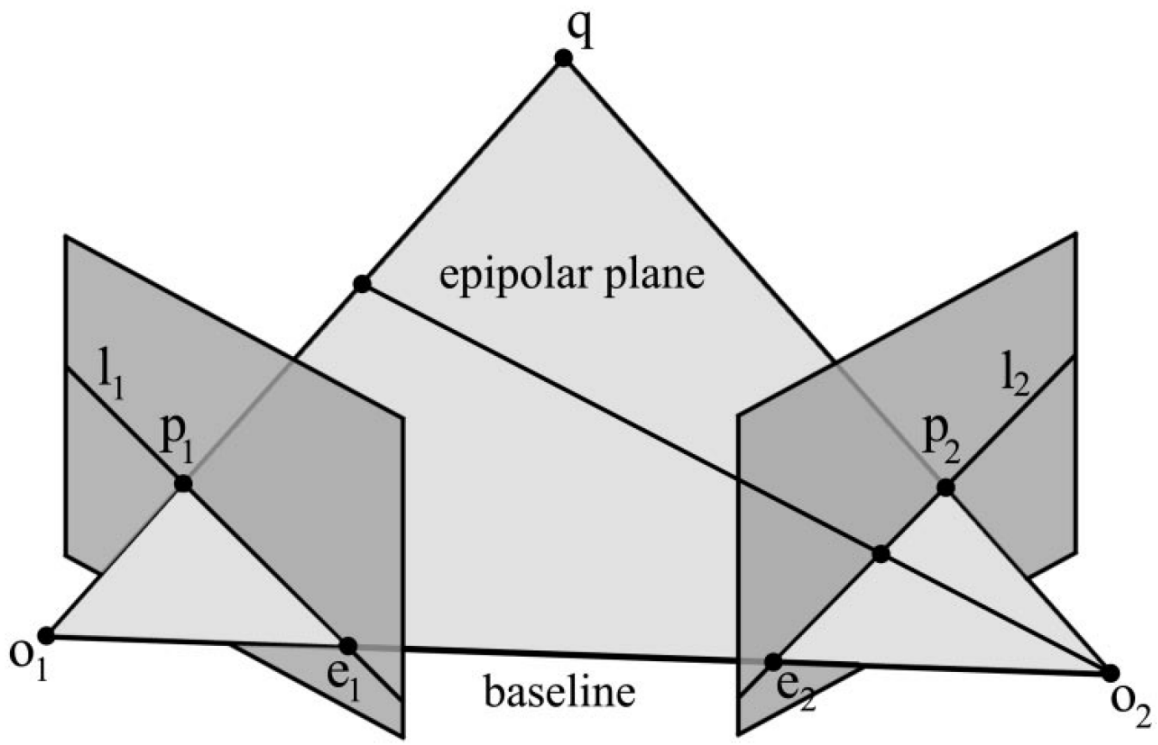

Figure 4. Epipolar Geometry [4]

q, o_1 (the focal point of the first camera), and o_2 (the focal point of the second camera) [10]. The plane must then intersect the first camera's image plane at some point p_1 and e_1 and as well as the second camera's image plane at some point p_2 and e_2. The goal then becomes determining what point p_2 corresponds to a given point p_1. To help determine p_2, the epipolar lines l_1 and l_2 are defined as the lines along which the epipolar plane intersects each camera's image plane. An epipolar baseline is then drawn as the line that connects the focal points of each camera and intersects the epipolar plane at points e_1 and e_2. Finally, point p_2 can be solved geometrically if the epipolar baseline, camera focal lengths, and depths of the points are known. the geometric relationship between p_1 and p_2 ultimately relates the position of q in 3D space to the cameras.

www.manaraa.com

2.5 Camera Calibration

Camera calibration is a process that finds the intrinsic and extrinsic properties of stereo cameras. The intrinsic properties are the focal length and the principal point location specific to an individual camera. The extrinsic properties are the properties that correspond to both stereo cameras, such as the distance between each camera's focal point. More specifically, camera calibration determines the rotation and translation (epipolar baseline) from the first camera to the second camera, allowing the corresponding points in each camera's image plane to be found.

The method for camera calibration is given by Zhang in [11]. Zhang's method begins with taking images of patterns with known dimensions. An example of a good pattern is a checkboard, where the length of each square box on the checkerboard is constant and the length is a known value. For this process to work, multiple images should be taken from each camera with the checkerboard at different orientations. The corners of each square can then be visibly matched between the corresponding images from the two cameras at specific pixels. Having multiple images at multiple orientations reduces the error that the pixels chosen as the corners from the two camera's images are not the exact same point in 3D space. In [11], Zhang also describes how to mathematically find the rotation matrix and translation vector between the two cameras from the matched corners in the images. An example of images taken for calibration for this research are shown in Figure 5.

2.6 Image Rectification

Image rectification is the process of rotating corresponding images from the two cameras such that the epipolar lines become horizontal [8]. If comparing multiple points on the same images, then multiple epipolar lines will then appear horizontal and parallel to each other. Image rectification is useful because it simplifies the feature

www.manaraa.com

(a) Left Stereo Image **(b) Right Stereo Image**

Figure 5. Stereo Images from a Left and Right Infrared Camera

matching process by using the parallel lines to match features between the images. The center of the rectified images is also useful as a reference point for centering the 3D reconstruction between the cameras. At this stage, the camera calibration and rectified images can be used to reconstruct the pixels of each image into points in 3D space. The collective reconstructed pixels then forms a point cloud in 3D space.

2.7 Registration

From the standpoint of AAR, images of the receiver being refueled are captured and the reconstructed point cloud represents the receiver. The receiver point cloud is called the sensed model. However, the sensed model is simply a set of (x, y, z) position vectors at this point. The data from the sensed model needs to be turned into a pose estimate of the receiver. Registration is the process of matching 2D or 3D objects using features [8], or in this case using the point cloud's individual points. Registration helps determine a pose estimate by taking a reference model of the object and matching it to the sensed point cloud. The resulting pose of the reference model is the pose estimate of the object. In the case of AAR, the object is the receiver.

One mathematical process for completing registration is through an Iterative Clos-

www.manaraa.com

est Point (ICP) algorithm. An ICP algorithm can work by either matching the sensed point cloud to the reference point cloud or vice versa. Since the reference point cloud is matched to the sensed point cloud in this research, this is the perspective that will be used. First, each point in the reference point cloud is compared to each point in the sensed point cloud to find the closest point. After the closest point is found for each point in the reference point cloud, the rotation and translation between the points is found. The root mean square (RMS) distance between each of the nearest points is also calculated as the error. The rotation and translation that reduces the RMS error from the current RMS error is then applied to all of the points and the process is repeated. The registration is complete when the RMS error cannot be reduced any further. Although a solution may be found, the solution may be a local minima for the RMS error and not the global minima, which is the most accurate answer. Symmetrical objects are good examples of objects that can have local minima errors during registration. About the axis of symmetry, the object may be incorrectly oriented while having a RMS error local minima that prevents the error from being corrected. Examples of ICP implementations are given by [12, 13, 14].

2.8 Truth Sources

Modeling the physical world is a difficult process and has error associated with it. For example, the lenses on the stereo cameras may distort the resulting images. Therefore, correction needs to take place to eliminate distortion error. The camera calibration process can also introduce error if the checkerboard corners are not perfectly aligned in the calibration. Therefore, the sensed model could have rotation and translation error associated with it. Ideally, error is recognized and reduced to 0. Nevertheless, it is important to compare the pose estimate for the sensed model with a truth source for the receiver's pose. Truth sources themselves may have known

www.manaraa.com

error, but the truth source's known error allows one to quantify the total error of the system.

2.9 Previous and Related Work

In the past two decades, much research has been done to solve the AAR problem and many solutions have been offered. In [15], Thomas lists various methods that have been researched to solve the AAR problem, such as using radar, GPS, vision navigation, electro-optical systems, and systems that combine more than one of these approaches. These solutions have eliminated parts of the AAR problem, however, no solution has completely solved the AAR problem. In this section, the previous research conducted on the AAR problem and the work related to the research in this thesis will be discussed.

Simulation Environments.

Some of the earliest AAR research began with setting up simulation environments for modeling the AAR problem and using the simulation to discover solutions to the problem. Although many AAR researchers use simulation environments to research specific solutions, the authors in [16, 17] used their simulation environments as general testbeds for solving the AAR problem. These simulation environments were important for modeling the AAR problem and gathering information on the problem. In [18], An used a simulation environment as well, however, An's main focus is on a UAV's relative position-holding while being refueled.

GPS and INS.

One of the most common solutions to estimating pose for the AAR problem is using a combination of GPS and Inertial Navigation Systems (INS) with a Kalman

www.manaraa.com

filter for filtering the signals. Some early work in the realm of AAR used only GPS in their solutions. Ross uses GPS in [19] to gather a Differential GPS (DGPS) solution between the tanker and receiver and to improve aircraft control. Dibley [20] also used relative GPS but used it for real-world probe-and-drogue tests by sending the calculated relative GPS solution from the tanker to the receiver. Additionally, Dibley found success using relative GPS during the real-world tests.

In [21], Williamson uses a combination of GPS and INS with an Extended Kalman Filter (EKF). Williamson then combines the GPS/INS solution with electro-optical sensors for an improved result. Liu [22] additionally provides methods for using GPS/INS with a Kalman filter as a solution. Similar to [21, 22], Johnson [23] simulates an INS with an EKF and combines that solution with simulated stereo vision to find a pose estimate that does not rely on GPS. Zhu [24] also searched for a solution that did not require GPS by complementing a GPS/INS with an EKF solution with an Infrared Search and Track (IRST) solution.

LiDAR.

Light Detection and Ranging (LiDAR) is another method used by researchers to either find a pose estimate of the receiver or to guide a receiver to the tanker. In the case of [25], Chen uses a 3D flash LiDAR camera to detect the drogue for a probe-and-drogue refueling scenario. Once the drogue is detected, the receiver can be guided to the drogue using the information from the LiDAR. Curro [26] also uses LiDAR to aid in navigation but does not limit the research to the probe-and-drogue method for refueling.

www.manaraa.com

Features and Markers.

Another popular solution to the AAR problem is using features or markers for guiding a receiver to a tanker. Although most feature/marker solutions use a simulation environment, Deng [27] uses binocular vision from a small handheld drone to evaluate position using markers on the handheld receiver drove. The computer algorithms in [27] use the sensed markers on the top of the receiver drone and output a position that can be used for navigation. Duan [28] also used markers on the receiver, however, Duan used real physical cameras pointed at screens to capture imagery of a receiver in a simulation environment. In [29, 30, 31, 32, 33, 34], the researchers use a mono vision camera on the receiver to either detect corners on the tanker or detect various types of markers placed on the tanker. Xin [35] uses a similar approach but instead uses an infrared mono camera to detect features. And in [36], Valasek uses a sensor on the receiver to detect visual beacons on the drogue for a probe-and-drogue refueling.

Stereo Vision.

Just as stereo vision is the focus of this research, others have also used stereo vision to compute pose estimates of the receiver. In Parson's work [7], Parson uses stereo cameras on a tanker to estimate the pose of the receiver in a 3D virtual world. Paulson [37] uses an approach similar to [7] but focuses on mitigiating the effects of the boom occluding the receiver for boom refueling. For both [38, 39], real-world stereo cameras combined with computer vision were used to find pose estimates of a receiver. In [38], Seydel created flight paths with a handheld drone and computed the pose estimate of the drone from the stereo vision imagery. Seydel also used Vicon chamber data for the drone as a truth source for validating the pose estimate. Stuart [39] also used stereo vision but used it with both electro-optical and infrared stereo

www.manaraa.com

vision. Additionally, Stuart was able to capture real imagery of an aircraft in-flight. However, Stuart's truth source for evaluating the pose estimates was only accurate to within 1.5 feet and Stuart was not able to evaluate the infrared imagery due to complications.

2.10 Discussion on Previous Work Methods

Although GPS has been shown to work as a solution to the AAR problem, the focus of this research is on finding a solution that does not depend on GPS. In certain environments, GPS may not be available, so the ideal solution to the AAR problem is one that works in any environment. Additionally, many previous researchers have focused their research on the probe-and-drogue refueling method. As stated earlier, this research is related to the boom method due its ubiquitous use by the Air Force. And finally, solutions that use features or markers are not considered due to the tremendous burden it would place on the Air Force to retrofit its fleet.

www.manaraa.com

III. Methodology

To make AAR a possibility, real-world tests must be conducted. And although it may not be possible to gather real tankers and receivers for the tests, the tests must resemble an aerial refueling as closely as possible. In preparation for the future AAR flight test, experiments were prepared and conducted with the flight test in mind. All hardware and software for the stereo vision system were designed to be used for the flight test with minimal or no changes. Pseudo refueling experiments were completed on the ground using the entire stereo vision system to evaluate the system and ensure its capability for the AAR flight test.

3.1 Stereo Vision System

At the heart of the stereo vision system are the stereo cameras. In an attempt to match stereo vision systems used on next-generation tankers, separate stereo vision systems comprised of stereo electro-optical (EO) cameras and infrared (IR) cameras were used as the stereo vision cameras. Using both EO and IR cameras increases the variability of the experiments and provides multiple data collection sources for analyzing. Additionally, the use of IR cameras provides the opportunity to validate stereo IR cameras as a viable option for stereo vision in the AAR domain.

Allied Vision® Proscilica GT1290C EO cameras were chosen for the EO stereo vision system. The GT1290Cs capture 24-bit RGB images at a resolution of 1280x960 and have adjustable focal points and aperatures. The adjustable focal point has the advantage of setting the focus to infinity to maximize image clarity for objects at a distance, since a receiver being refueled will be at a distance of greater than 30 meters prior to contact with the refueling boom. Additionally, the cameras will not auto focus, which would interfere with the camera calibration. Since the flight test is

www.manaraa.com

a day-time flight test, the adjustable aperature enabled the aperature to be closed to its maximum closure in preparation for the flight test.

The IR cameras chosen for the IR stereo vision system were two long-wave infrared (LWIR) cameras. The image resolution for the IR cameras is 1024x768 and the images produced are 16-bit grayscale PGM images. Like the EO cameras, the IR cameras were also focused to infinity. And although the image resolution of the EO and IR cameras is not the same, both stereo pairs have the same 16:9 aspect resolution and 56 degree field of view. Both the GT1290C EO cameras and the IR cameras are capable of capturing imagery at a rate of 30hz. Additionally, both sets of cameras are equipped with gigabit network outputs that interface with gigabit ethernet. The gigabit outputs are important for being able to transfer up to 30 images per second. When an image is captured, it is transfered via the gigabit output to a data collection computer where it is saved.

Figures 6 and 7 show the EO and IR stereo cameras. In Figure 7 the cameras are mounted to a bracket. This bracket is the same bracket that is used for the future flight test. The bracket mounts to the underside of the C-12 to capture imagery at a downward look angle conducive for refueling. The downward look angle provides the ability to view the receiver aircraft from a perspective near the boom. The bracket was machined for a 0.5 meter baseline between each camera pair. Therefore, the IR cameras are 0.5 meters apart and the EO cameras are 0.5 meters apart. The expected epipolar baseline after camera calibration is then 0.5 meters for each camera pair.

3.2 Trigger Board

Even though the cameras are capable of capturing images at 30hz each, the stereo cameras act independently and will not capture the images at the exact same time. However, camera calibration and image rectification requires image pairs to be cap-

www.manaraa.com

Figure 6. From the Left to the Right: Left IR Camera, Left EO Camera, Right IR Camera, Right EO Camera

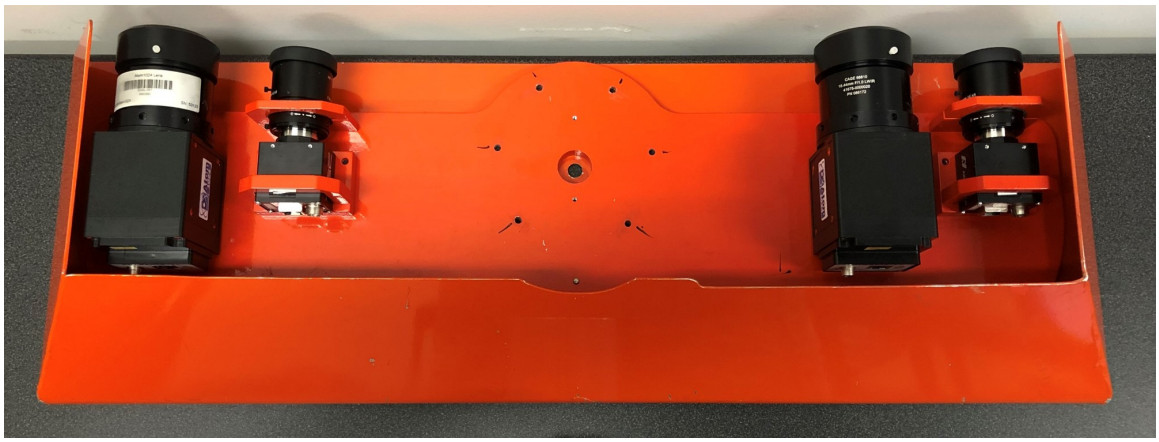

Figure 7. Cameras Mounted to Test Bracket in the Same Order as Figure 6

tured at the exact same moment. Otherwise any change in the image plane of the cameras between captured images will result in error. The solution is to send a 30hz pulsed signal to each camera at the same time and to trigger an image capture when a pulse's edge is received by the camera. Therefore, all 4 cameras will maintain a synchronized 30hz image capture rate.

The pulsed signal was created through the use of a trigger board specifically built for the flight test. The trigger board is designed to receive an RS-232 serial input signal from an FTDI USB cable connected to the data collection computer. Prior to capturing images, the cameras are connected to the trigger board by coax cables with BNC connections on the trigger board. When ready to collect imagery, the

www.manaraa.com

data collection computer's CPU transmits the serial 30hz signal through the FTDI USB cable to the trigger board. The trigger board then sends the 30hz pulsed signal to each of the cameras to capture images. Although the IR and EO stereo systems are independent from each other, each stereo system receives the same pulses and triggers at the same time. Each set of images is also timestamped with the CPU time, which allows the IR and EO images to be compared for data analysis based on their timestamp.

Figures 8 and 9 show the trigger board and coax trigger cables respectively. Both the trigger board and trigger cables were designed to specification for the flight test.

Figure 8. Trigger Board with FTDI USB Cable and Power Adapter

Figure 9. Coax Trigger Cables for Each Camera

3.3 Calibration

The imagery captured is only useful if the cameras are calibrated, providing the ability to extract features and 3D points from the rectified images. A metallic checkerboard with 30 millimeter square tiles provided the means for calibrating the cameras.

www.manaraa.com

One set of tiles used the metal surface of the board as the tile. The other set of tiles used a white heat insulating paint. On the back of the checkerboard is a black painted surface that absorbs IR heat. The checkerboard was specifically designed in this manner so it could be used to calibrate both the IR and EO cameras at the same time. To the EO cameras, there is a clear color distinction between the metal tiles and the white paint tiles. To the IR cameras, the metal tiles would emit a bright heat signature due to the black backing and the white paint tiles would appear nearly heat-less. Therefore a contrast existed between the tiles for both the IR and EO images.

For calibration images, it is not useful to use the 30hz pulsed signal because the total number of images would amass quickly. Instead a software module was utilized that used the FTDI drivers to only send a pulse on the FTDI cable upon key press via the data collection computer. The key press method provided an easy way to move the checkerboard to different positions and orientations and capture an image when ready. A sample of the calibration images taken for each camera is shown in Figure 10. For reasons discussed later in this chapter, the cameras are angled at an upward direction for the calibration images. However, the upward angle made it difficult to capture images with the checkerboard covering the entire image plane for each camera. Therefore, the camera calibration quality may not have been as accurate as possible. Error in the camera calibration is further discussed in the Results chapter.

The intrinsic and extrinsic parameters were calculated for each stereo vision system using the MATLAB® Camera Calibration Toolbox. Within the Camera Calibration Toolbox, MATLAB® offers an app named the Stereo Camera Calibrator, which is specifically designed for stereo cameras. The Stereo Camera Calibrator takes a set of images from the left camera and the corresponding set of images from the right camera as input. Additionally, the 30 millimeter length of each checkerboard tile is

www.manaraa.com

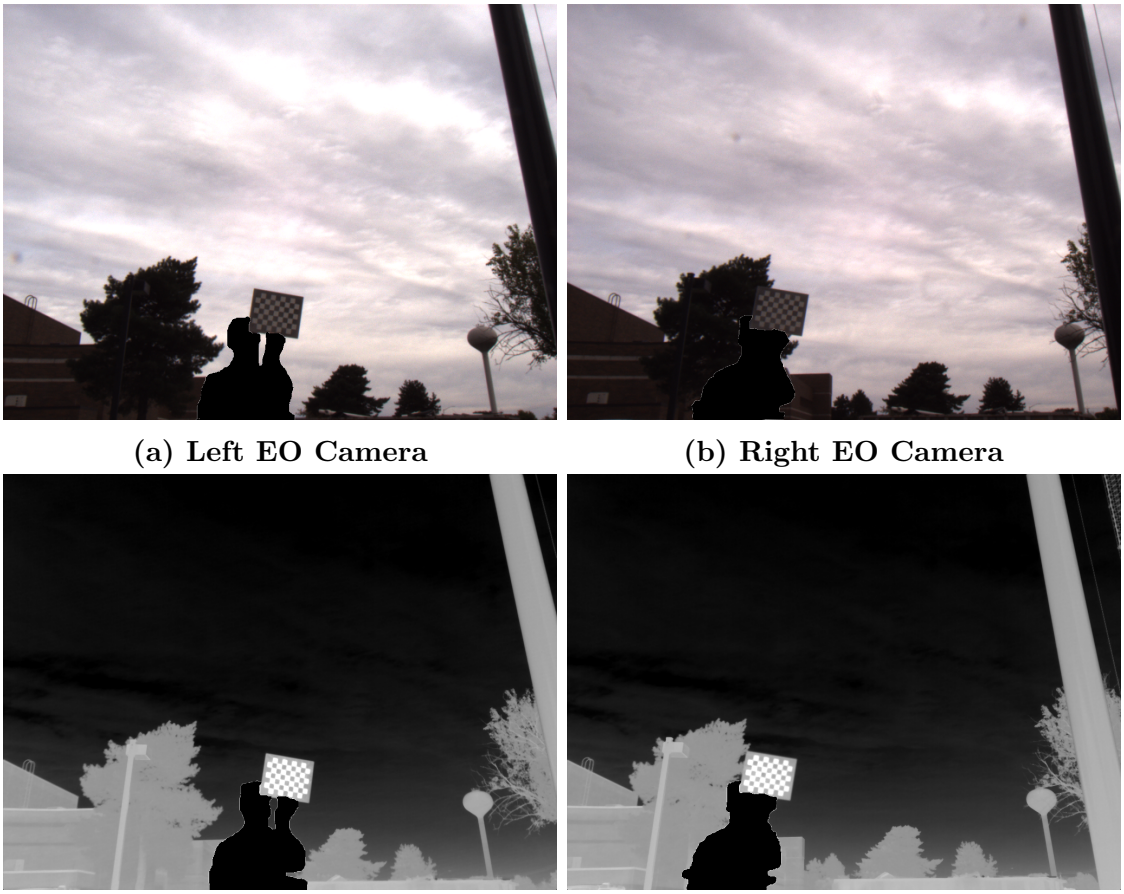

(a) Left EO Camera **(b) Right EO Camera**

(c) Left IR Camera **(d) Right IR Camera**

Figure 10. Calibration Images for EO and IR Cameras

input. The Stereo Camera Calibrator then finds the checkerboard tile corners for each image and calculates the pixel error for the images as seen in Figure 11. Finally, the intrinsic and extrinsic parameters are calculated and exported.

3.4 Truth Source

Creating a pose estimate of a receiver is only useful if there is a truth source to validate the estimate. To produce accurate orientation and position truth data for the psuedo receiver that is used during experiments, the Geodetics, Inc. Geo-RelNAV® system was utilized. The Geo-RelNAV® system creates a differential orientation and DGPS solution between a Primary system and Secondary system. Both the Primary

www.manaraa.com

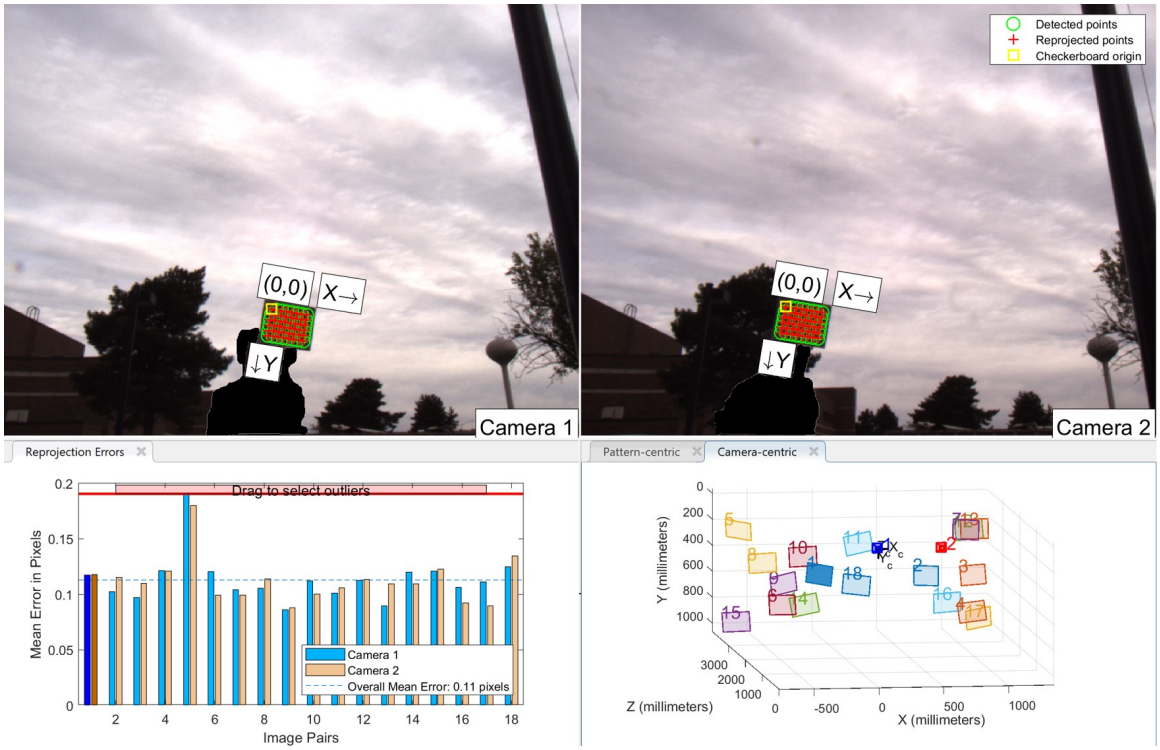

Figure 11. MATLAB ® Stereo Camera Calibrator Output for EO Cameras

and the Secondary systems are equipped with their own KVH1750 Inertial Measurement Units (IMU) and GPS units. The KVH1750 uses a Laser Ring Gyroscope to collect IMU data and the GPS data is collected through a GPS antenna. Together, the IMU and GPS data is used to calculate the pose truth data via a tightly coupled EKF. The Primary and Secondary systems both collect and save their IMU and GPS data for processing. The Secondary system, identical to the Primary system, is shown in Figure 12.

Prior to using the Geo-RelNAV® system, the Primary and Secondary systems must be calibrated. Each unit must receive GPS signals from the GPS signal for approximately 1 minute before it has a fix on the GPS position from the satellite constellation. The KVH1750 IMU is initially required to be coarse aligned. Coarse alignment is an initial attidude estimate made by each unit after the IMU has been held stationary for approximately 1 minute. After coarse alignment is achieved, the

www.manaraa.com

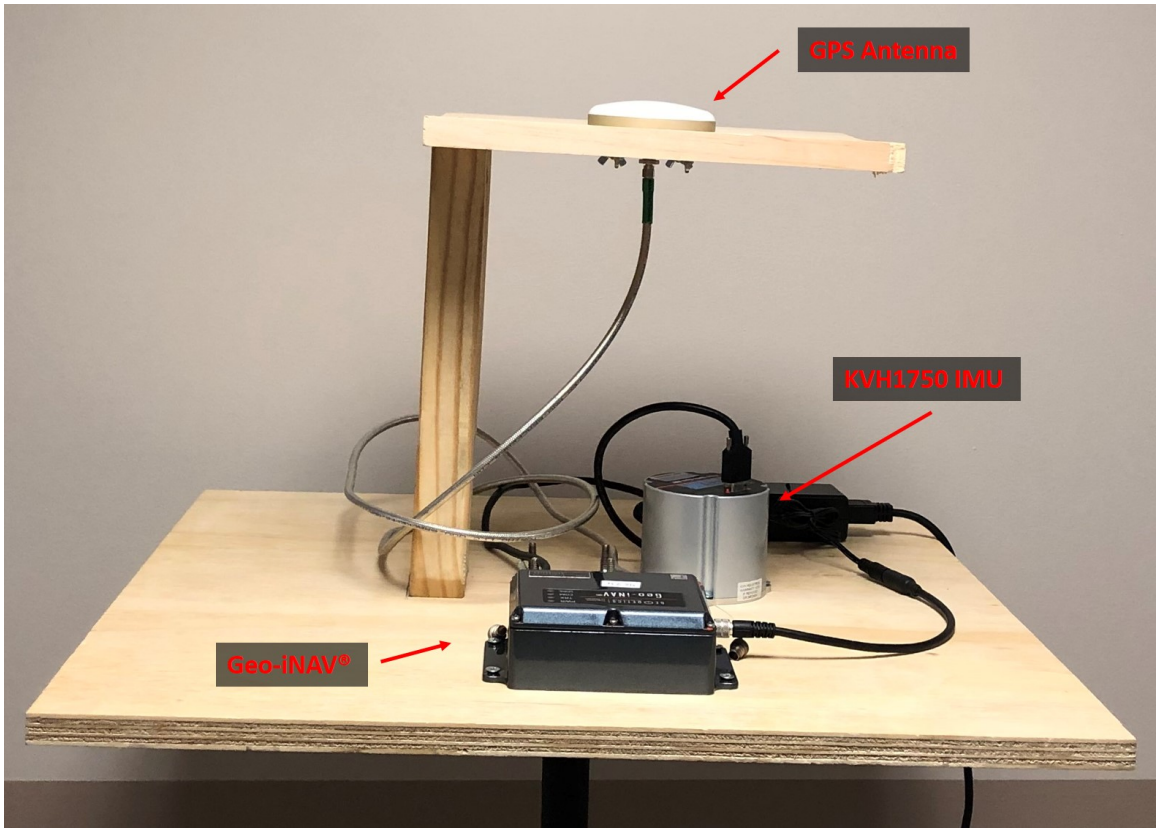

Figure 12. Secondary Geodetics Geo-RelNAV® System

IMU must be fine aligned. Fine alignment requires the IMU to be moved at a steady fast-walking pace while making yaw movements. The yaw movements are accomplished by moving in approximately 15x15 meter rectangular patterns. Fine alignment typically finishes after completing 3-4 of the rectangular patterns. Once fine alignment is complete, the attitude output from the IMU is highly accurate but the solution may drift over time if the IMU does not move or is moved with a constant bias. The Geodetics software shown in Figure 13 shows the attitude output from the IMU after fine alignment has completed. The top right box in the figure shows a top-down view of the rectangular patterns that were traversed. Additionally, the Geodetics software will indicate when a GPS fix is acquired and when coarse and fine alignment are complete via th *Quality* value in the bottom left of the figure.

A contributing factor to using the Geo-RelNAV® system was its high level of ac-

www.manaraa.com

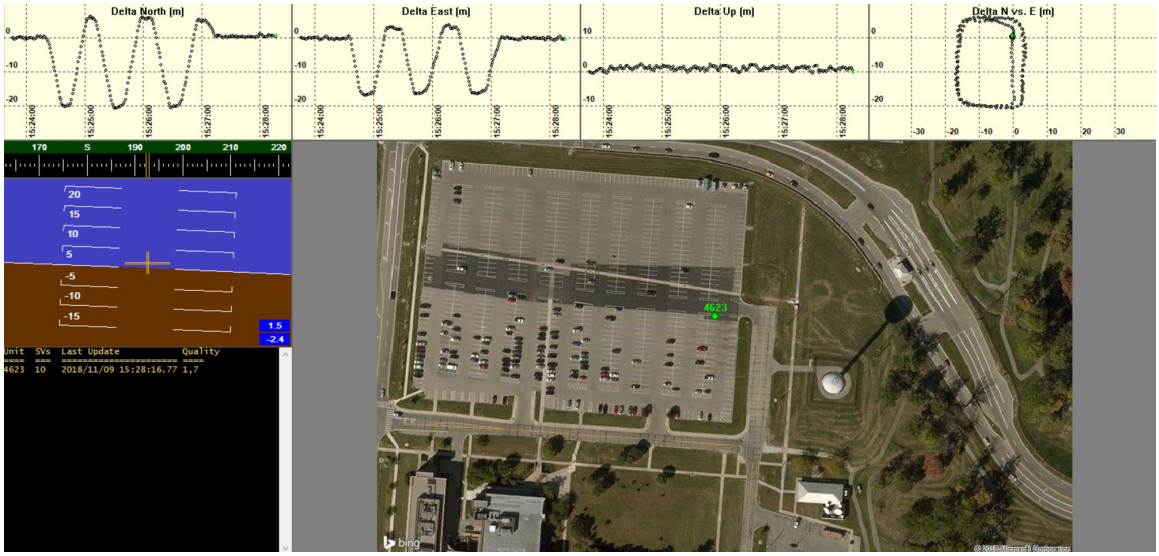

Figure 13. An Attitude Recording of the Primary Geo-RelNAV® System after Fine Alignment

curacy. The GPS portion of the system is advertised to have a 5cm/10cm GPS error for L1/L2 respectively when used in differential mode [40]. And the IMU portion has an advertised 0.01 degree to 0.05 degree error for differential solutions [40]. Because the GPS antenna and IMU are not co-located, the Geo-RelNAV® system must account for the difference in position between the GPS and IMU. The Geo-RelNAV® system accounts for this difference by using the measured (x, y, z) lever-arm vector between the GPS antenna and the IMU and computing all data relative to the IMUs position.

All data collected for the experiments was done using the system in differential mode, which is the mode the system will use for the flight test. The differential orientation and position solutions are calculated by post-processing through filtering techniques completed by Geodetics, Inc. For the data collected in the experiments, the GPS data was collected at 10hz and the IMU data was collected at 100hz.

www.manaraa.com

3.5 GPS Time Server

The accuracy of the Geo-RelNAV® system is useless if the pose data from the sytem is not time aligned with the imagery taken from the stereo vision systems. Therefore, each image needs to be time stamped with a GPS time that correlates to the GPS time for the each data point in the truth pose data. The time stamping is accomplished using a TM2000A time server made by Time Machines Corp. The TM2000A time server receives GPS signal using a GPS antenna and supports the Precision Time Protocol (PTP) and Network Time Protocol (NTP). The protocols are used to turn the TM2000A into a time server with GPS time.

Prior to collecting imagery, the data collection computer is connected to the TM2000A via ethernet. Once connected, the internal clock for the data collection computer is synced with the GPS time hosted on the TM2000A. The data collection computer can then be disconnected from the TM2000A, however, the internal clock then relies on its own accuracy to keep its clock time close to GPS time. When first synced, the data collection computer's clock is accurate to within 10^{-6} seconds. Once synchronized to 10^{-6} seconds, the data collection machine's Xeon processor is assumed to not drift by more than 1/30 of a second over the 2 hours of image collection. The TM2000A itself is handheld in size and requires a power connection to operate.

3.6 Pseudo Tanker

A successful pseudo refueling experiment depends on properly establishing a pseudo tanker and pseudo receiver. The refueling experiments are conducted on the ground, therefore, the pseudo tanker was designed using a wagon that could securely support the vision system, the data collection computer, the Primary Geo-RelNAV® system, and a power supply system. Additionally, the GPS antenna was placed above all of the equipment to prevent the blocking of GPS signals traveling to the GPS antenna.

www.manaraa.com

Figures 14 and 15 show the pseudo tanker with the IMU axis attached.

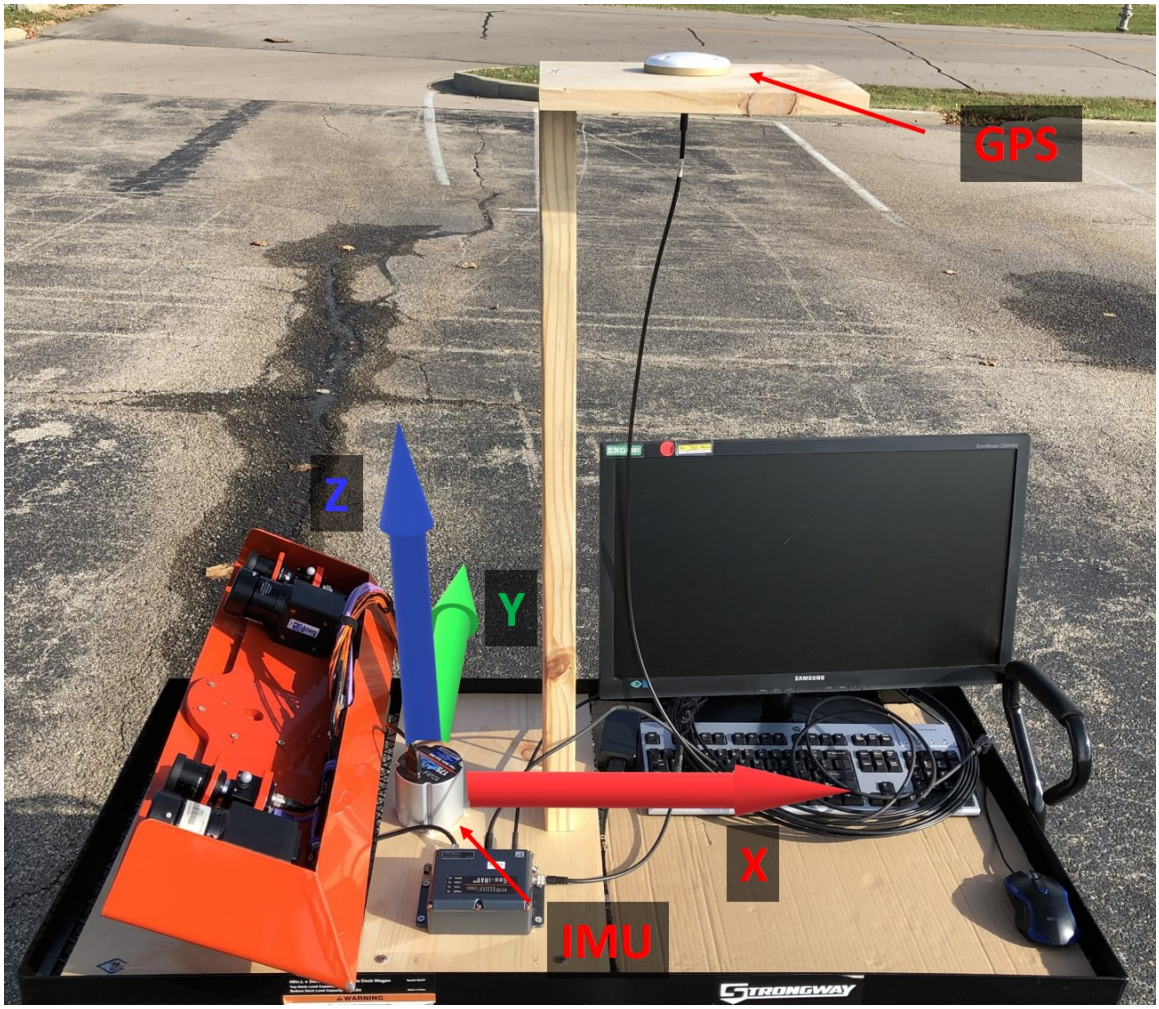

Figure 14. Rear View of Pseudo Wagon Tanker with Primary IMU Axis

As noted previously, the cameras are angled upward. The upward angle was deliberately designed to increase the amount of sky shown in the background of the images. Having the sky in the background is important for reducing the number of features in the images from the ground. This setup also attempts to better replicate an aerial refueling operation since the receiver is surrounded by the sky during the refueling. Additionally, the ground shown in the background of aerial refueling images is a great distance from the receiver itself.

www.manaraa.com

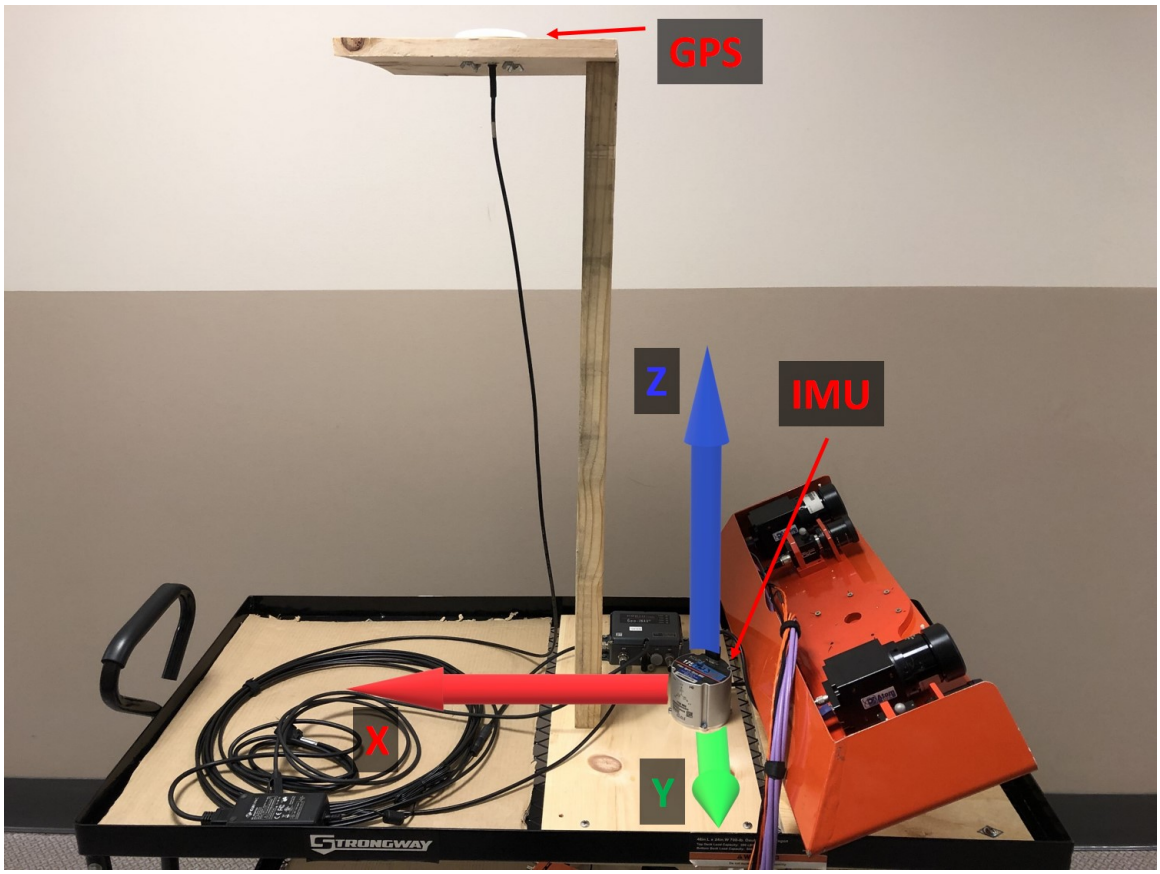

Figure 15. Side View of Pseudo Wagon Tanker with Primary IMU Axis

3.7 Pseudo Receiver

The next step in the design process was to develop a pseudo receiver for the ground experiment. Since the cameras on the pseudo tanker are angled upward, the pseudo receiver needed to be hoisted up into the air to be shown in the image plane of the cameras. The pseudo receiver was designed using another wagon, but with a wooden platform lofted into the air using steel pipes. The platform was needed to secure the Secondary Geo-RelNAV® system on the receiver. The receiver was then designed with a pseudo wing and pseudo body using wood boards. After various pattern designs for the wing and body, a random shapes pattern was affixed to the wing and body to increase feature detection in the images. The random pattern replicates the fact that a receiver aircraft has various corners, painting, rivets, and other features

www.manaraa.com

for detection. Otherwise, the boards by themselves did not produce many features. Figures 16 and 17 show different views of the pseudo receiver. Refer to Figure 12 for an up-close view of the Secondary Geo-RelNAV® system on the pseudo receiver.

Figure 16. Front View of Pseudo Receiver

When a receiver approaches the tanker with a constant approach, the look direction of the stereo vision system will intersect with the receiver at an angle. Therefore, the wing on the pseudo receiver was intentionally angled so the look direction of the stereo cameras on the pseudo tanker would intersect the pseudo receiver wing at an angle throughout an experiment. Figure 18 shows an example of camera look directions from a tanker and the pseudo tanker. The specific angle was not modeled because the angle of intersection with the receiver is not always going to be the same angle for every refueling approach. The pseudo receiver's wing was simply modeled

www.manaraa.com

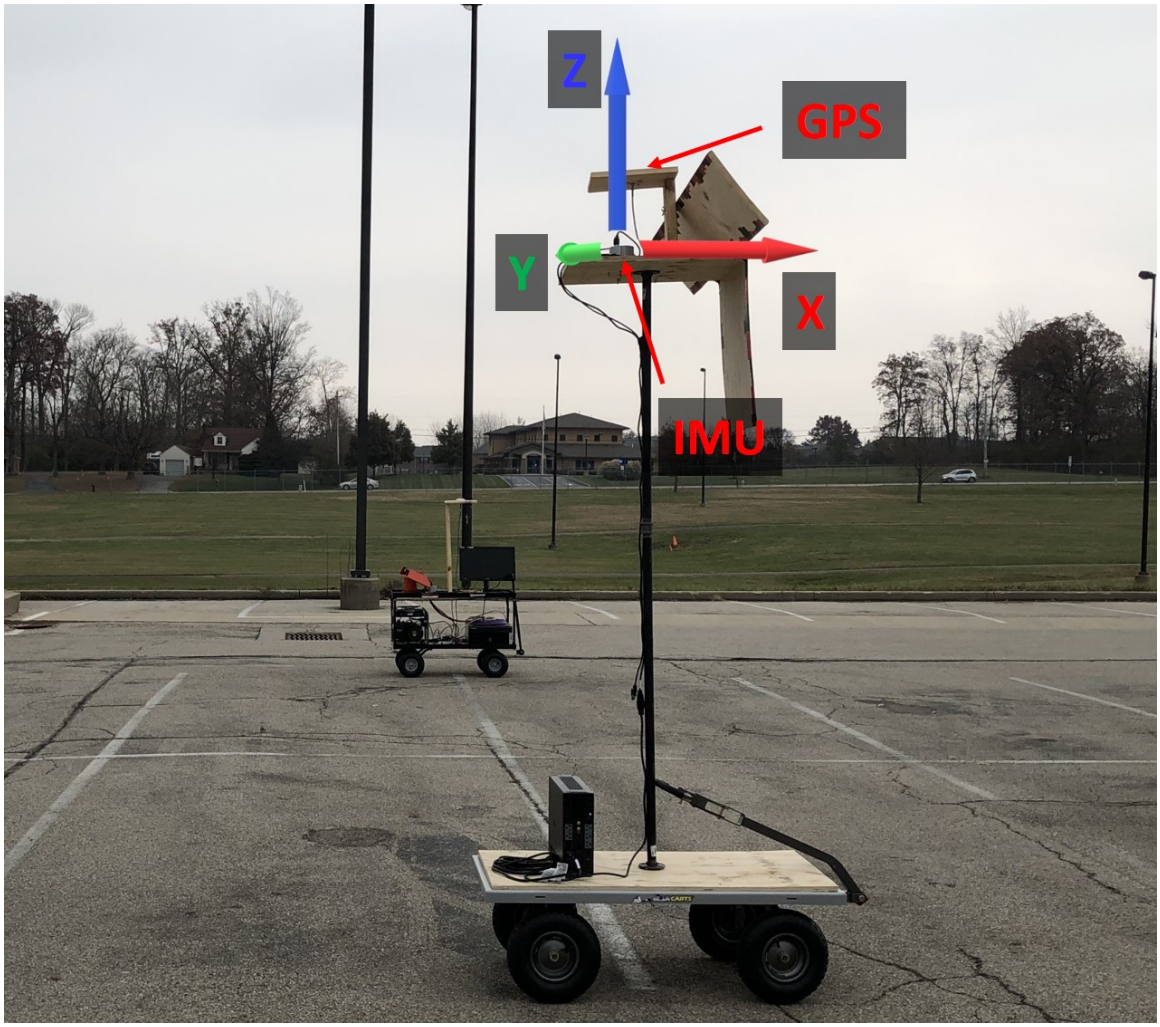

Figure 17. Side View of Pseudo Receiver with IMU Axis

to have an angle of intersection because a tanker's cameras will intersect the receiver at an angle during an aerial refueling.

3.8 Experiments

The actual experiments were completed in a parking lot with an open field in the field of view from the cameras. The pseudo tanker was set on one end of the parking lot with the stereo vision cameras' look direction facing the pseudo receiver. In total, 8 test runs were completed. For each test run, the pseudo tanker remained

www.manaraa.com

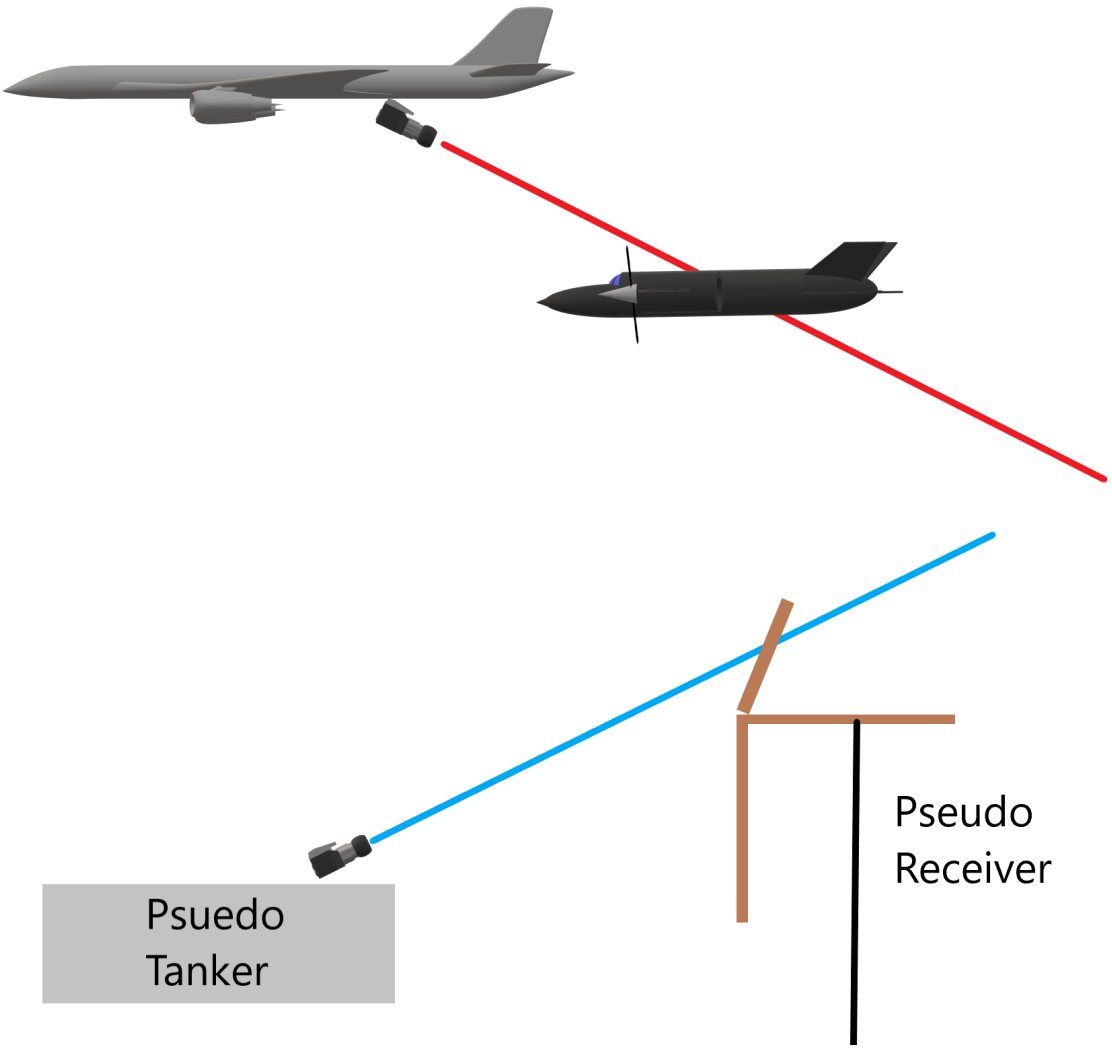

Figure 18. Camera Look Directions and Receiver Intersection

stationary while the pseudo receiver approached the pseudo tanker. Throughout approach, the stereo vision system captured imagery of the pseudo receiver and save the Geo-RelNAV® data. Figure 19 shows a general top-down view of the experiments that were completed. Figure 20 shows a view of the pseudo receiver during the first test run.

For the first 6 test runs, the pseudo tanker remained in the exact same position. Table 1 shows the approaches that were made for the first 6 test runs. The pseudo tanker was moved to a different position for the final 2 test runs to gather data from

www.manaraa.com

Figure 19. General Outline of Experiments

a new position. Table 2 shows the approaches that were made for the final 2 test runs.

Test Number	Pseudo Receiver Approach Pattern
Test 1	Approach in the receiver's +x direction
Test 2	Approach in the receiver's +x direction, then reverse to -x
Test 3	Zig-zag towards pseudo tanker
Test 4	Same as Test 2
Test 5	Approach in the receiver's +x, -y direction
Test 6	Approach in the receiver's +x, +y direction

Table 1. Pseudo Receiver's First 6 Test Approaches

Test Number	Pseudo Receiver Approach Pattern
Test 7	Approach in the receiver's +x direction
Test 8	Approach in the receiver's +x direction

Table 2. Pseudo Receiver's Final 2 Test Approaches

www.manaraa.com

Figure 20. View of the Pseudo Receiver Approach from the First Test Run

Image Processing.

With all of the data collected from the experiments, the imagery could be processed to create a pose estimate of the pseudo receiver. The image processing began with the use of OpenCV. OpenCV is an open source Computer Vision Library [9]. OpenCV provides many functions for processing imagery. The primary functions used for processing the images were the rectify and stereo block matching functions. Figure 21 shows sample images from both the EO and IR stereo vision systems from the first test run. As previously noted, the apertures on the EO cameras were closed to the maximum closure which is why the images appear dark.

Using the calculated intrinsic and extrinsic calibration parameters, the OpenCV rectify function rotates the image pairs to rectify the epipolar lines. Along the epipolar lines, the OpenCV stereo block matching function matches features along the epipolar lines and creates a disparity map. The disparity map is an image that uses a black-to-white scale for the pixels in the dispartiy map. The white pixels indicate features

www.manaraa.com

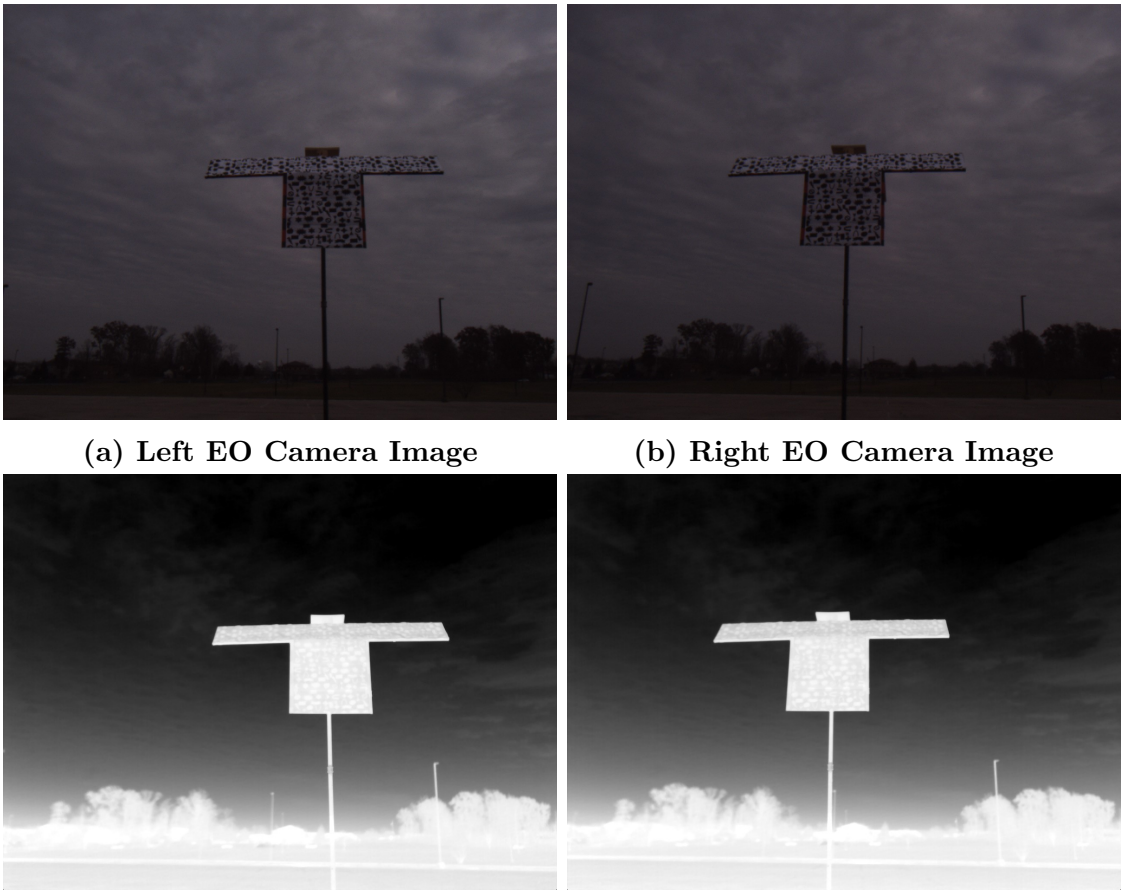

(a) Left EO Camera Image **(b) Right EO Camera Image**

(c) Left IR Camera Image **(d) Right IR Camera Image**

Figure 21. Stereo Images from Test 1

that were matched with high parallax and are closer to the camera than dark pixels, which are features that were matched with low parallax. The dispartiy map in Figure 22 shows the pseudo receiver close to the camera, as the near-white pixels show the outline of the pseudo receiver. Therefore, the calibration parameters and disparity map provide a means to map each disparity map pixel into a 3D point cloud.

3.9 Virtual World

From the standpoint of computer vision, each point from the point cloud has its own position vector in (x, y, z) coordinates that can be modeled in 3D space. Modeling the experiments in a virtual world provides many benefits. First, it provides

www.manaraa.com

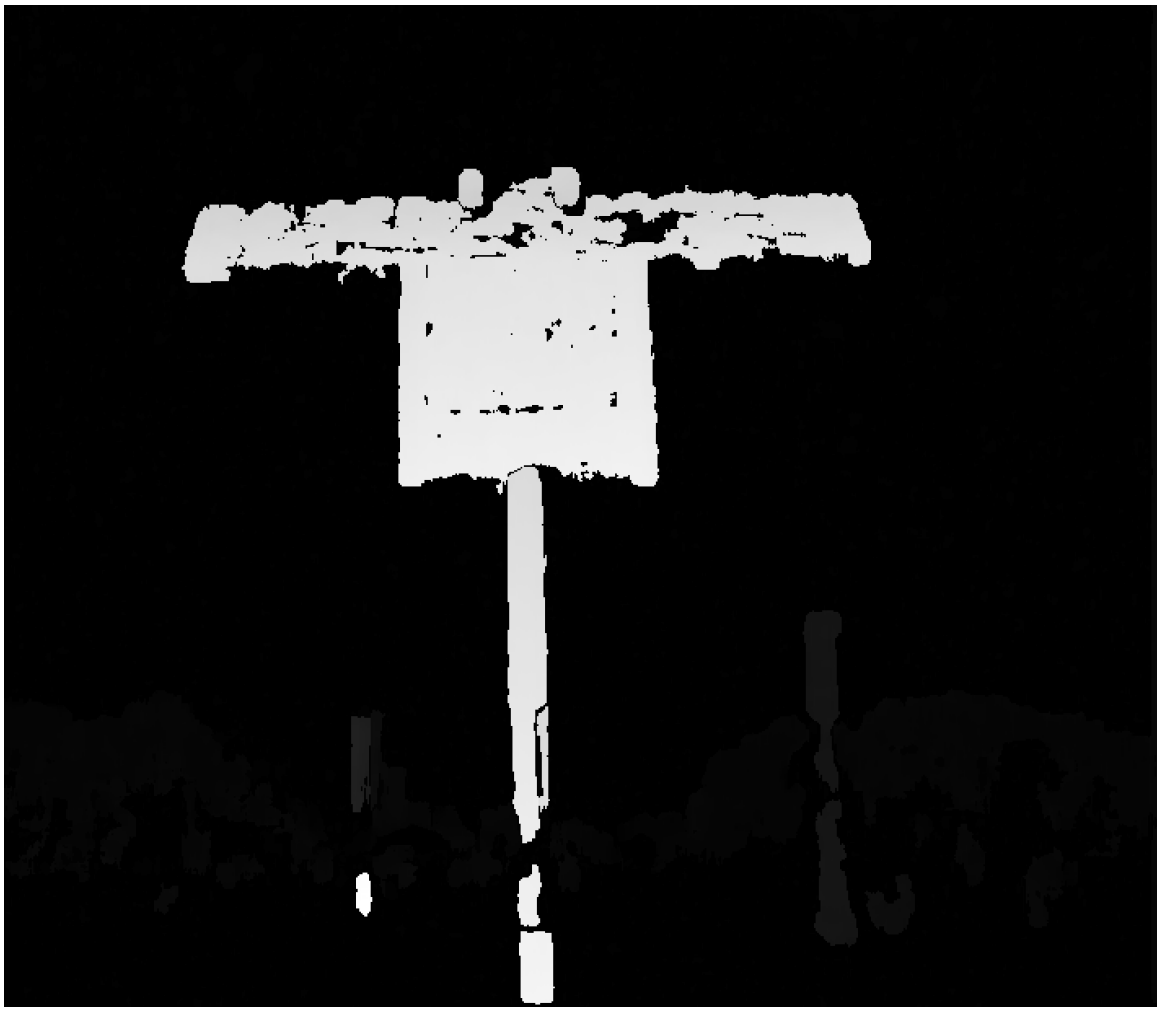

Figure 22. Disparity Map from the First Test Run using IR Imagery

a way to visualize the experiment and visualize aspects such as the registration. Second, the virtual world is a simulation environment that can deterministically re-execute the experiments as many times as necessary, provided the computing power is available. The virtual world also improves the ability to make statistical analysis of the experiments, improving the feasibility of error correction. If the experiments experienced any errors from a constant bias, the bias can be adjusted in the data and the experiment can be corrected in the virtual world. Lastly, a set of images taken over time can be reconstructed as a point cloud in real-time in the virtual world, rendering the scene in real-time in the same manner as when the images were

www.manaraa.com

captured.

The experiments were modeled in the virtual world using the AFTR Burner engine, which is based on the engine in [41]. Rendering in the AFTR Burner engine is done using OpenGL. Since each experiment was completed in the parking lot, the scene in the virtual world was set to show the parking lot via satellite imagery combined with elevation data. The coordinate frame for the terrain was expressed in the ECEF frame and the Geo-RelNAV® position data was converted to ECEF. Therefore, the virtual models could be placed in the virtual world to appear exactly as they did in the real world. Figure 23 shows the virtual world with the models from the experiment.

Figure 23. Virtual World View of the First Test Run

www.manaraa.com

Modeling.

To simulate the experiments in an exact manner in the virtual world, each aspect of the experiment was modeled with 3D models. The 3D models were created using Blender, which is an open source modeling software package [42]. Although the virtual world is unit-less, all of the virtual models have dimensions modeled in meters. Therefore, all points in the virtual world are relative to meters. The pseudo tanker was modeled with the stereo vision system and its IMU. In the virtual world, the pseudo tanker is positioned using the Geo-RelNAV® data relative to the IMU on the virtual model, making the virtual model appear in the same location in the virtual world as its physical counterpart was in the real world. The same process was completed for the pseudo receiver as was done for the pseudo tanker. The primary difference between the virtual world and the real world was that the wagon portion of the pseudo tanker and pseudo receiver were not modeled. Modeling the wagons was not necessary since the receiver was the focus of the imagery. Figure 24 shows the pseudo tanker and pseudo receiver as modeled in Blender. It is important to note that the pseudo receiver model is used as the truth source and its pose is driven by the Geo-RelNAV® truth data.

Another important aspect of modeling the experiment in the virtual world was appropriately modeling the virtual camera frusta. In the virtual world, the position of the 3D reconstructed point cloud (sensed model) was relative to the center point between the stereo camera's focal points. The sensed model was positioned in this manner because the image rectification will center the reconstructed points between the camera focal points. The physical vector between the IMU and the center point between the cameras was measured so it could be modeled in the virtual world as an offset. The offset was used to place the center of the stereo cameras' frusta on the virtual pseudo tanker relative to the pseudo tanker's IMU, replicating the real-

www.manaraa.com

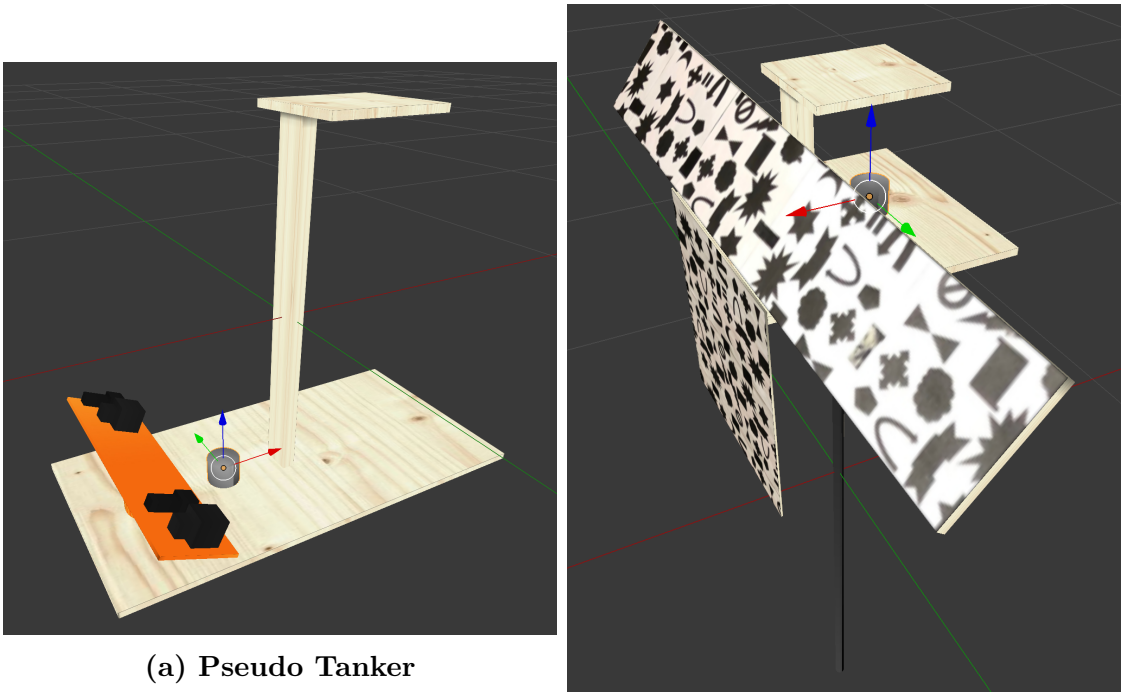

(a) Pseudo Tanker

(b) Pseudo Receiver

Figure 24. Models of the Pseudo Tanker and Pseudo Receiver in Blender

world setup. Since the IR and EO stereo vision systems have different center points between the camera's, the proper offsets for each stereo vision system were measured for processing their respective data.

Registration of Reference Model.

The final step before producing a pose estimate is registration. In order to accomplish registration, areference model of the pseudo receiver was created using only red 3D points, as shown in Figure 25a. Because the cameras primarily only see the front of the pseudo receiver, the reference model does not contain any points from the backside of the pseudo receiver. Additionally, the points for the pole were removed to best replicate an object in the air.

Because there are objects in each image other than the pseudo receiver, such as light poles, the sensed point cloud originally included points for all of these objects.

www.manaraa.com

However, it is assumed for an aerial refueling that there would be few, if any, other objects in the tanker's cameras' image frame. Therefore, the largest mass of points could be assumed to be the receiver and all other points would be removed from the sensed model. Under this assumption, a virtual box was constructed around the sensed receiver model using the truth data and all points outside of the box were removed from processing.The pole was removed from the sensed receiver model as well, since the pole was only used to enable the experiment in the first place. The sensed point cloud model of the pseudo receiver is shown as yellow 3D points in Figure 25b.

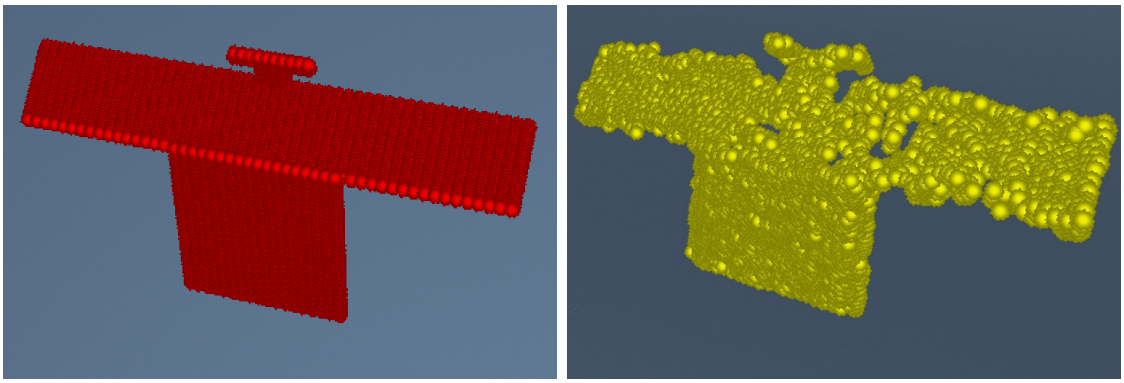

(a) Red Reference Point Cloud **(b) Yellow Sensed Point Cloud**

Figure 25. Reference Model and Sensed Model as Point Clouds

To finish the registration process, ICP needed to best align the reference model onto the sensed model. Since a receiver will approach a tanker with roughly the same look direction as the tanker, it was assumed that the reference model could initially set its orientation to the tanker's orientation before performing ICP. Orienting the reference model with the tanker minimized the chance of ICP converging on a local minima. When ICP completes, the pose of the reference model serves as the pose estimate for the pseudo receiver, providing a **solution** for the pose of the pseudo receiver. With the pose estimate "in-hand", the estimate can then be compared to the truth data. Figure 26 shows the reference point cloud matched to the sensed point

www.manaraa.com

cloud with the truth model in nearly the same orientation and position, indicating a good estimate.

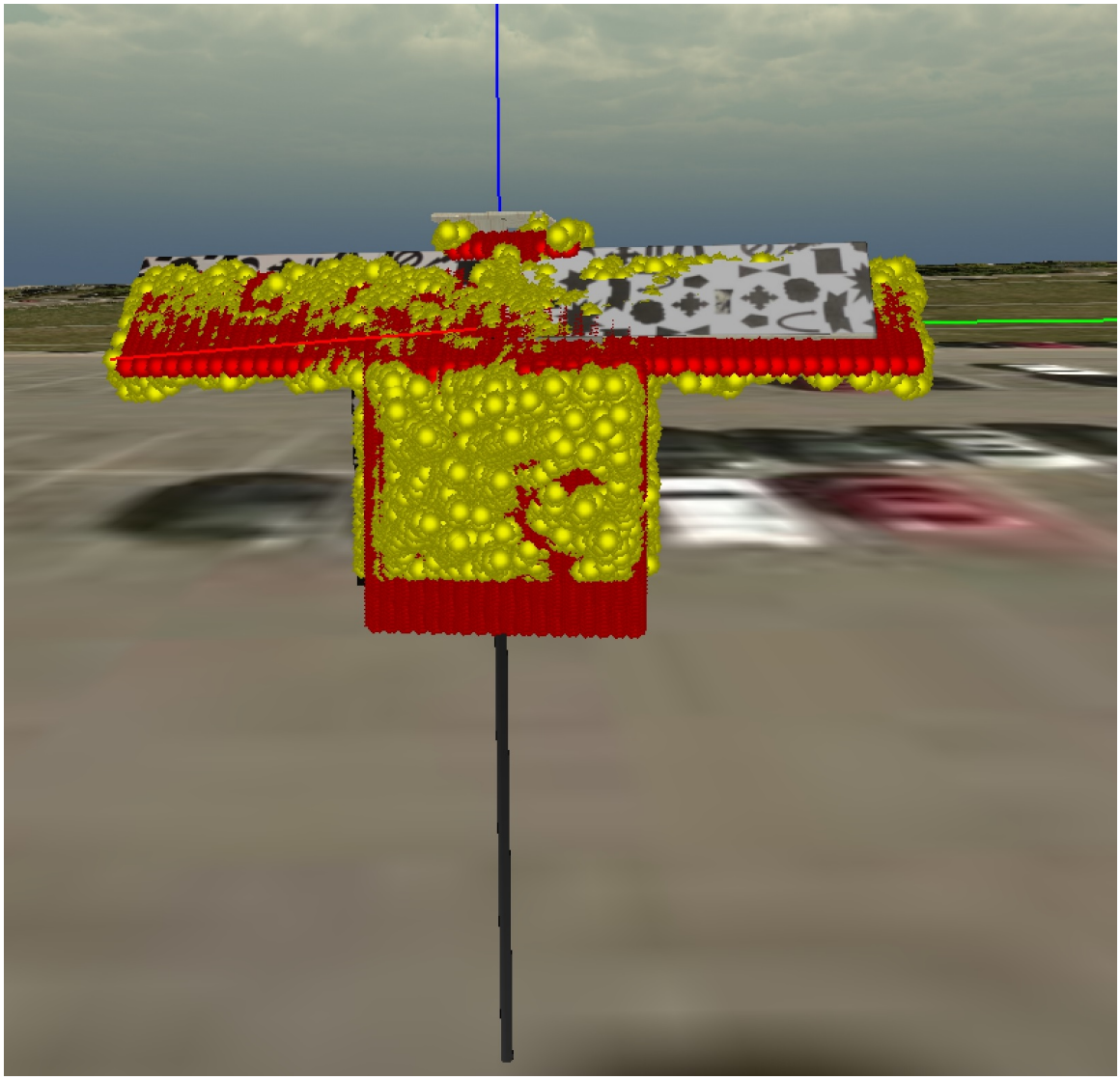

Figure 26. Registration of the Reference Point Cloud with the Sensed Point Cloud

www.manaraa.com

IV. Results

4.1 Comparison to Real-World Flight Test

The comparisons between the pseudo refueling experiments and a real aerial refueling would not be significant if the pose estimate is poor when the pseudo receiver is equidistant from the cameras to a real world receiver. Since the pseudo receiver is much smaller than the C-12 receiver that will be used during the flight test, an equivalence ratio must be developed to compare the two situations. For the purposes of holding the two situations equal, it is assumed that the C-12 receiver and pseudo receiver are centered on the horizontal field of view of left stereo camera on their respective tankers. It is also assumed that the contact point for the C-12 being refueled is approximately 30 meters from the rectified camera, which is centered between the stereo cameras.

The two refueling situations are compared by finding the ratio of each receiver's wingspan to the width of the horizontal field of view of the camera at a given distance d. For any angle θ for the horizontal field of view for the camera, the equation for finding the width of the horizontal field of view at a distance d is given by Equation 1 and shown in Figure 27.

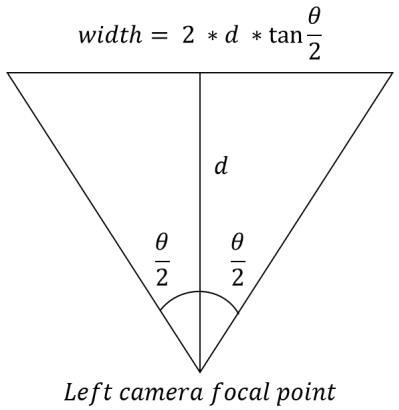

Figure 27. Width of Horizontal Field of View

www.manaraa.com

$$width = 2 * d * \tan\frac{\theta}{2} \tag{1}$$

The ratio of wingspan to width is then given by Equations 2 and 3.

$$equivalence\ ratio = \frac{wingspan}{width} \tag{2}$$

$$equivalence\ ratio = \frac{wingspan}{2 * d * \tan\frac{\theta}{2}} \tag{3}$$

Since θ will be held the same for both refueling scenarios, it is considered constant for the comparison. Equation 4 shows the final ratio with constants removed.

$$equivalence\ ratio = \frac{wingspan}{2 * d} \tag{4}$$

The C-12C is a re-purposed variant of the C-12A. The wingspan of the C-12A is 54 feet, 6 inches [43] which is equivalent to 16.16 meters. At a distance of 30 meters, the assumed contact point for the receiver, the *equivalence ratio* for the receiver is equal to 0.269, as shown in Equation 5.

$$equivalence\ ratio = \frac{16.16}{2 * 30} = 0.269 \tag{5}$$

Equation 6 is now used to find the distance at which the pseudo receiver's wingspan will appear equal to the C-12C's wingspan in the imagery.

$$d = \frac{wingspan}{2 * equivalence\ ratio} \tag{6}$$

The wingspan of the pseudo receiver is approximately 1.842 meters. Solving for Equation 6 yields a distance of 3.42 meters, as shown in Equation 7.

www.manaraa.com

$$d = \frac{1.842}{2 * 0.269} = 3.42\ meters \tag{7}$$

Therefore, the wingspan of the C-12C at a distance of 30 meters will appear similar in imagery to the wingspan of the pseudo receiver when it is at a distance of 3.42 meters. In general, this wingspan comparison provides a baseline for comparing the distances at which the objects appear relative to each other. Because the edge of a wing is not infinitely thin, the wing will always be visible during a horizontally centered approach. And although the bodies of the C-12C and the pseudo receiver are not compared, some portion of the receiver's body will also be visible at the contact point, providing additional features for stereo block matching.

The wingspan comparison is not perfect due to the fact that two pixels will map to features whose separation increases as object's distance increases from the camera. Therefore, the error will be greater for an object farther from the camera than an object closer to the camera, even if they appear as the same size in the image plane. One method of addressing this issue is to increase the resolution of the camera images, thereby decreasing the physical separation between features that map to individual pixels for an object at a set distance. However, even for the resolution of the IR cameras, 1024x768, the error increase would be minimal for an object 30 meters away. If a wing covered the entire image plane horizontally at a distance of 30 meters, the 1024 horizontal pixels would map to features approximately 3 centimeters apart. Even at a distance of 80 meters, the pixels would map to features that are approximately 8 centimeters apart. Therefore, the increased error due to distance would be minor given the resolution of the stereo cameras and the distance at which the a real aircraft would refuel.

For all results in this chapter, distance is measured from the left camera to the pseudo receiver's IMU. The error is provided as the 6 degrees of freedom (6DOF), the

www.manaraa.com

(x, y, z) position error and the roll, pitch, yaw (RPY) error. Additionally, the position error between the truth data and the pose estimate is given in the frame of the pseudo receiver's IMU. In this chapter, references to position error are based on when the pseudo receiver is 5 meters from the camera. Additionally, the IMU's reference frame (north-west-up) is not used for the RPY error. Instead, the RPY error is given from the pseudo receiver's IMU using a north-east-down reference frame. Lastly, only the results from the first 6 test runs are shown in this chapter.

4.2 Analysis of IR Imagery

For the IR cameras, Figures 28, 29, 30, 31, 32, and 33 RPY estimation error and Figures 34, 35, 36, 37, 38, and 39 show the position estimation error.

In general, the RPY error for all of the test runs was highly consistent. When at a distance between 10 and 5 meters from the camera, the pitch error was near or less than 5 degrees for each of the runs. However, the roll and yaw error were around 2 degrees or less. The RPY error in test run 4 is scattered when the pseudo receiver was near the camera due to the receiver going out of the frame of the camera. Overall, the IR RPY error was low and consistent across all of the test runs.

The position error was also relatively consistent. For tests runs with a steady approach (1, 2, and 4), the (x, y, z) error was around 10 centimeters or less when the distance was less than 5 meters. The y error was especially low, being nearly 0. The z error was consistently under 10 centimeters for all of the runs when near a distance of 5 meters and with the exception of test run 4, the x error was also around 10 centimeters or less. For test runs 5 and 6, the y error is higher than the other runs but the distance from the camera in test runs 5 and 6 is beyond 5 meters. The important takeaway is that the position error for (x, y, z) is below 20 centimeters for all of the runs.

www.manaraa.com

For test runs 2 and 4, the x error is different when the pseudo receiver is reversed compared to when it is moved forward. This is likely due to the fact that the pseudo receiver was reversed at a different angle than when moved forward, which would affect the consistency in the depth results. However, when traveling forward or in reverse, the results maintain a high accuracy. This phenomenon also occurs in the EO results, indicating consistency amongst the results.

4.3 Analysis of EO Imagery

For the EO cameras, Figures 40, 41, 42, 43, 44, and 45 RPY estimation error and Figures 46, 47, 48, 49, 50, and 51 show the position estimation error.

The results for the EO cameras were even better than for the IR cameras. The RPY error was also extremely consistent with the error being around 2 degrees or less for all of the test runs at distances near 5 meters. This RPY error in general is outstanding for AAR. The (x, y, z) error was also around 10 centimeters or less for all of the runs except test run 5 and test run 6. In test runs 5 and 6, the y error is near 15 centimeters. However, the distance in these tests is beyond 5 meters. Therefore, the y may have been lower had the pseudo receiver been closer to the camera. It should again be noted that the large amount of error near the camera in test run 4 is due to the pseudo receiver going out of the view of the cameras. For both the EO and IR results, the position error near 15 meters on tests 5 and 6 is due to the pseudo receiver nearing the edge of the image plane of the stereo vision system. Therefore, the results will be poor as the pseudo receiver moves out of the images.

www.manaraa.com

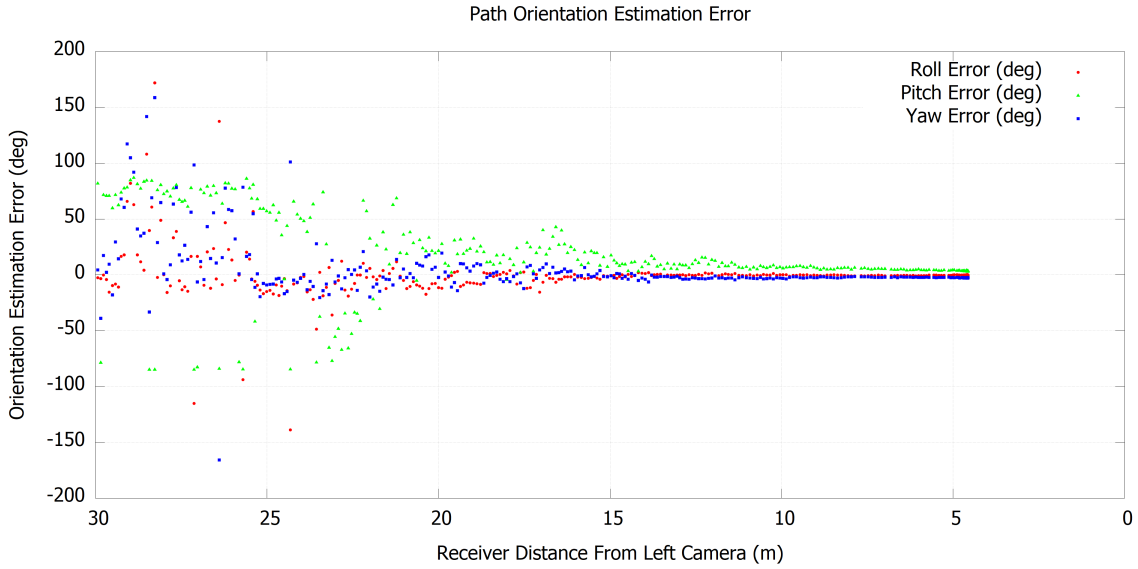

Figure 28. IR RPY Error for Test Run 1

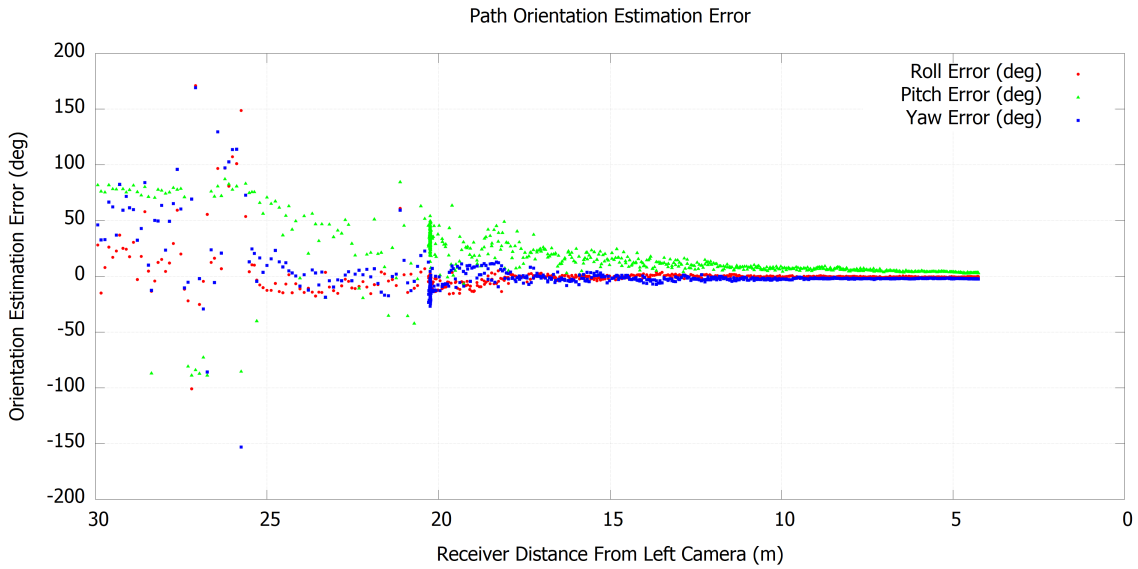

Figure 29. IR RPY Error for Test Run 2

www.manaraa.com

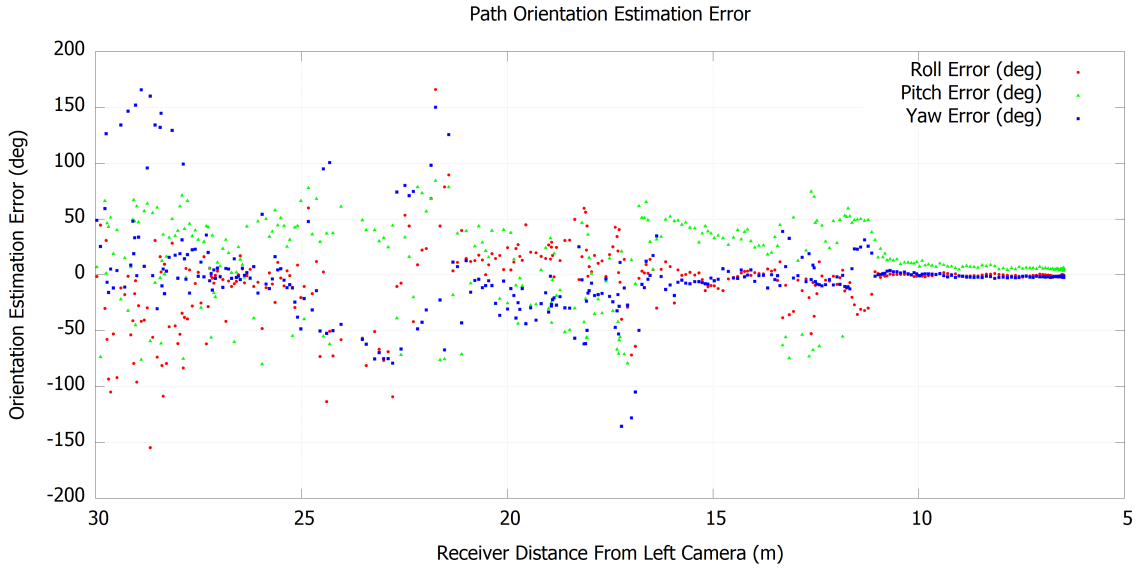

Figure 30. IR RPY Error for Test Run 3

Figure 31. IR RPY Error for Test Run 4

www.manaraa.com

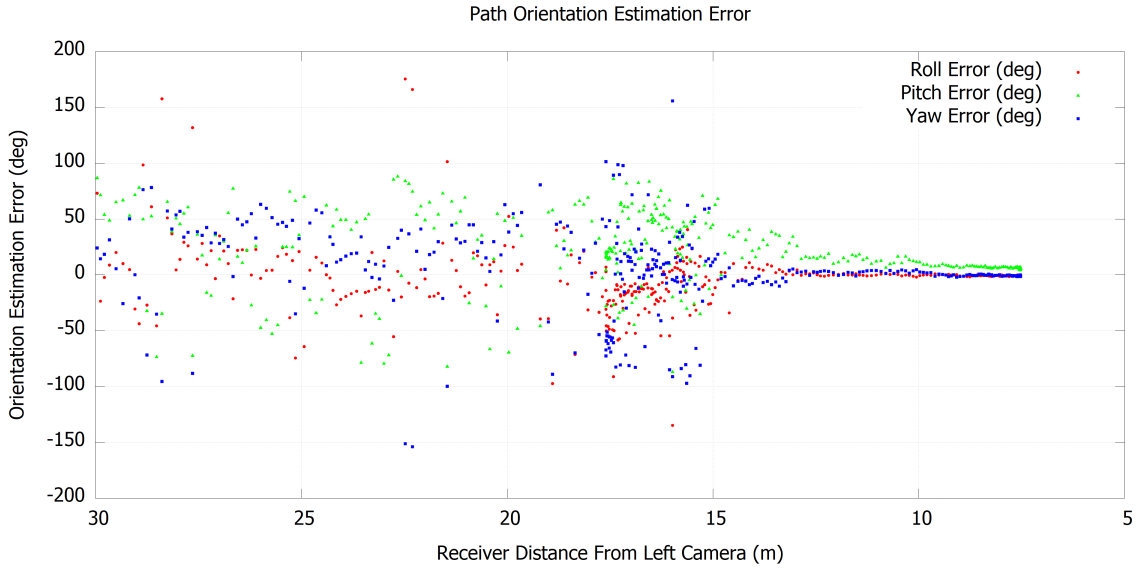

Figure 32. IR RPY Error for Test Run 5

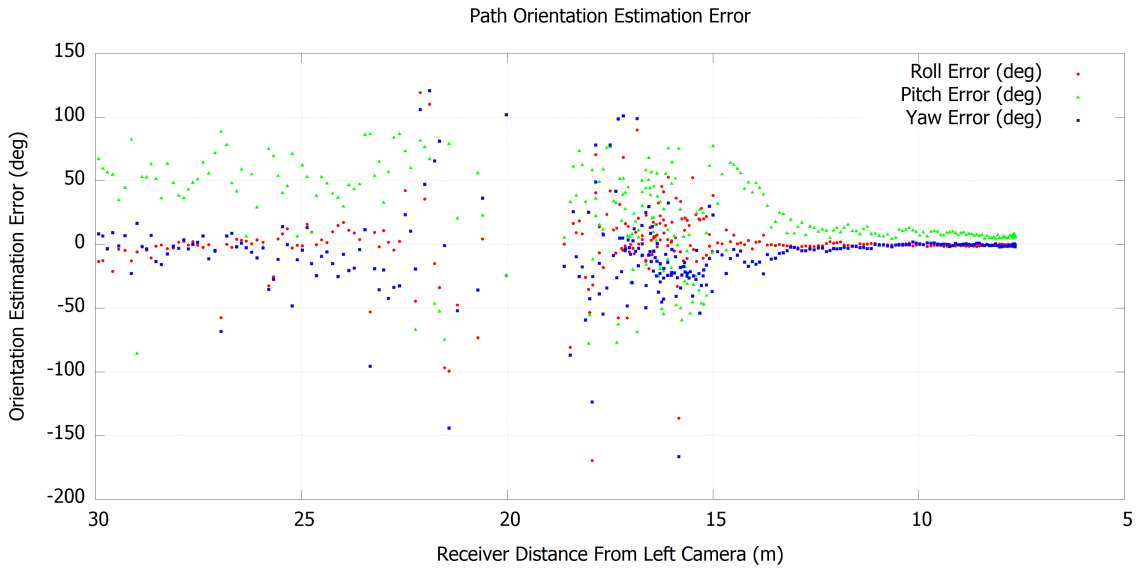

Figure 33. IR RPY Error for Test Run 6

www.manaraa.com

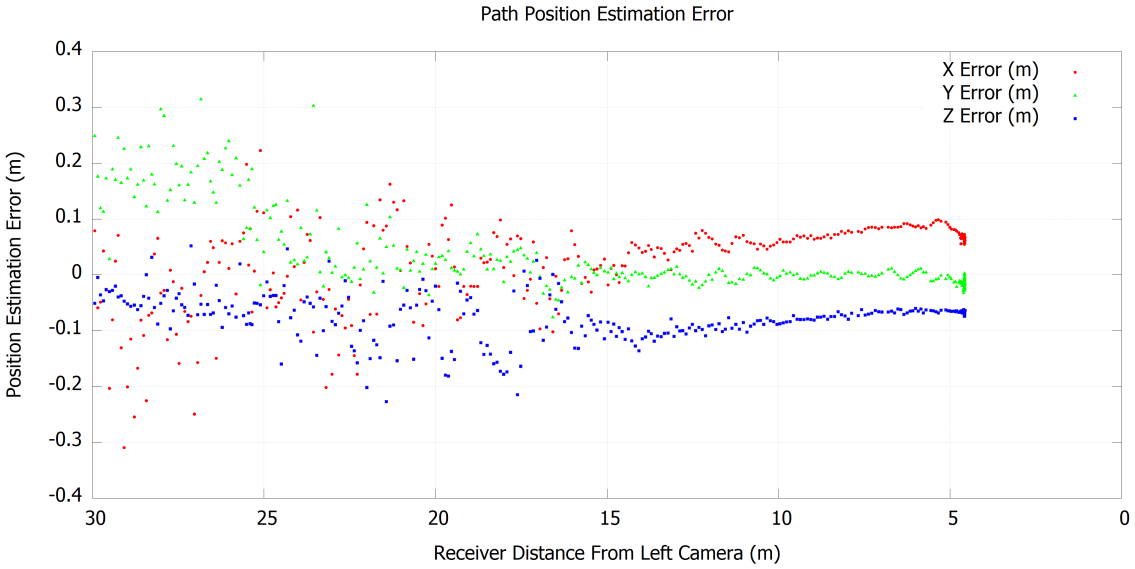

Figure 34. IR Position Error for Test Run 1

Figure 35. IR Position Error for Test Run 2

www.manaraa.com

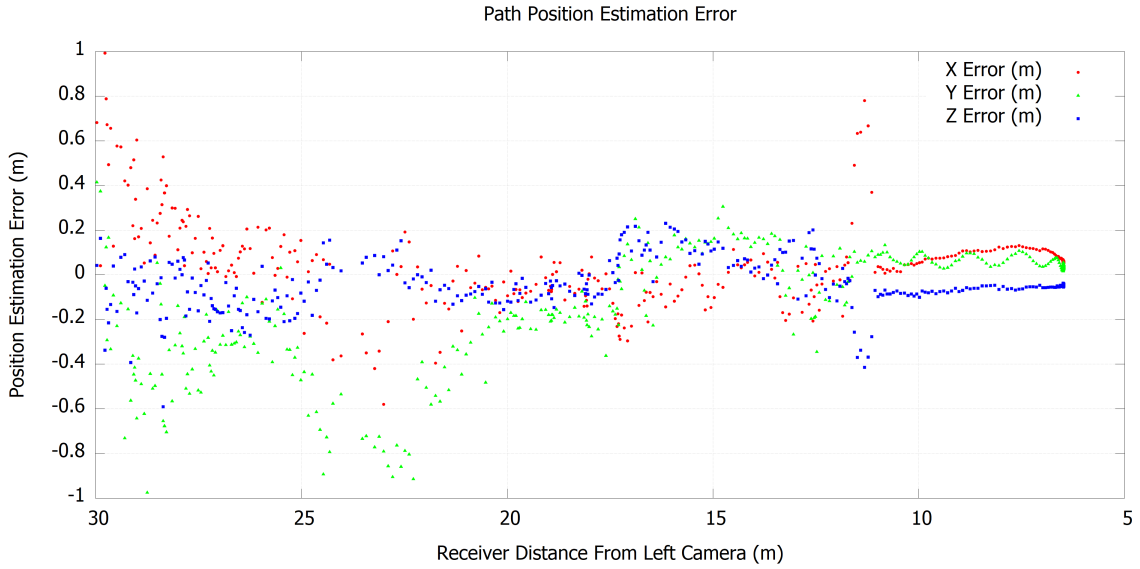

Figure 36. IR Position Error for Test Run 3

Figure 37. IR Position Error for Test Run 4

www.manaraa.com

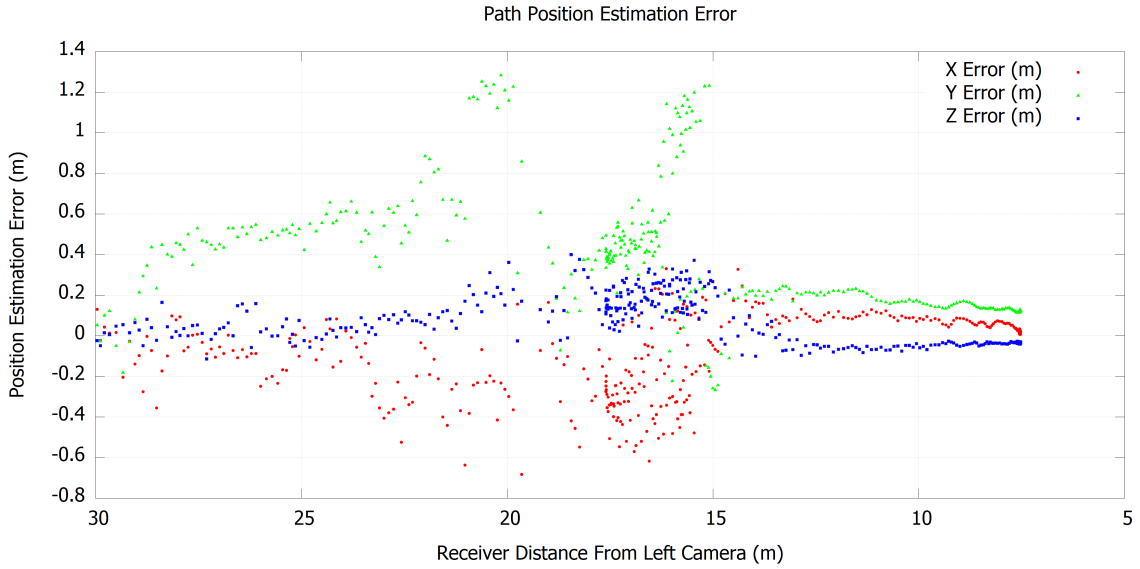

Figure 38. IR Position Error for Test Run 5

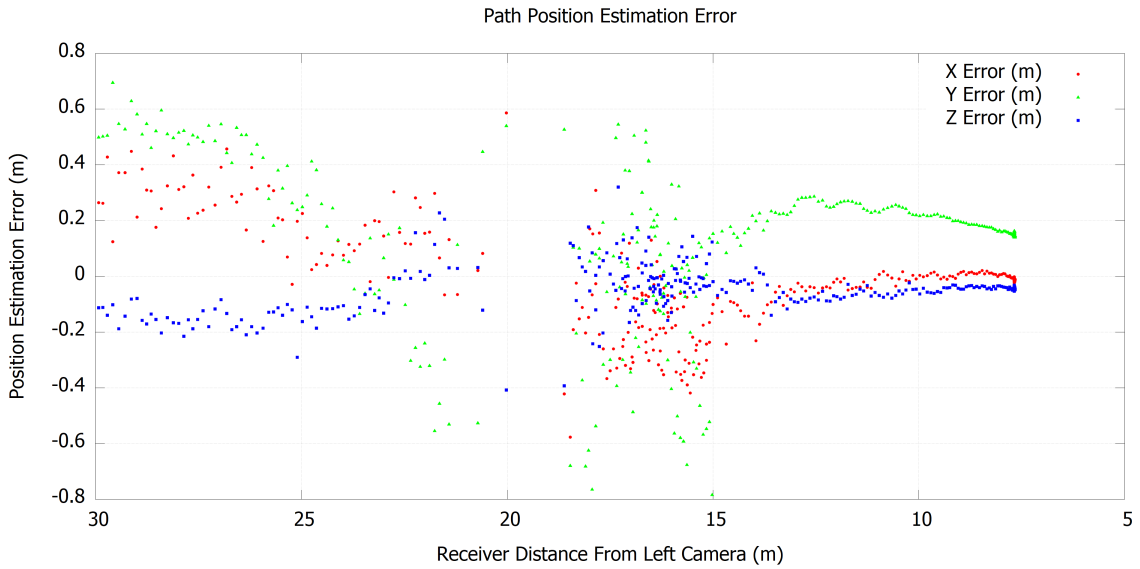

Figure 39. IR Position Error for Test Run 6

www.manaraa.com

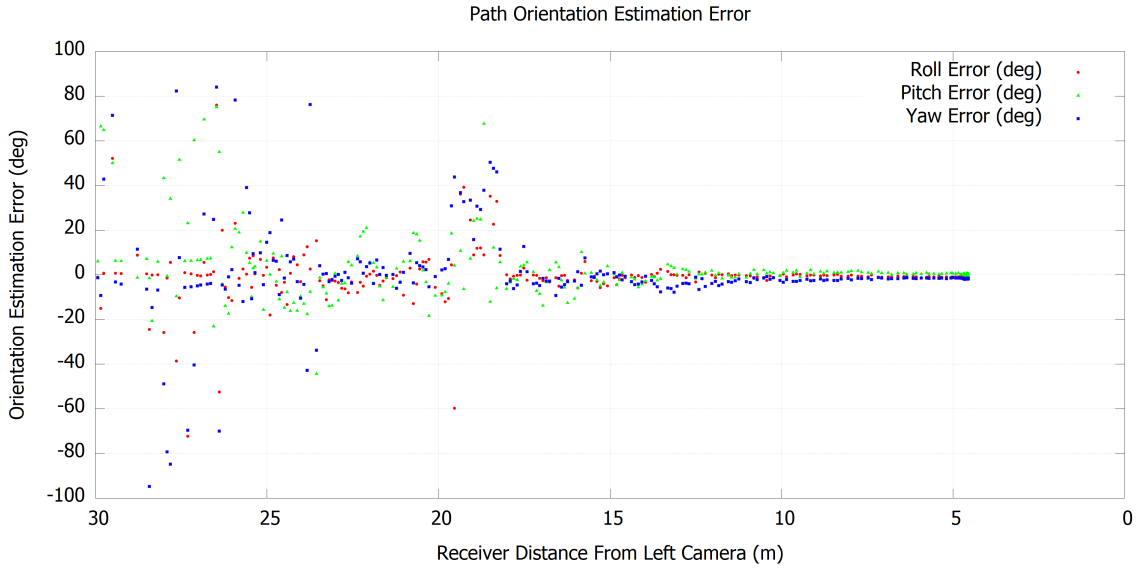

Figure 40. EO RPY Error for Test Run 1

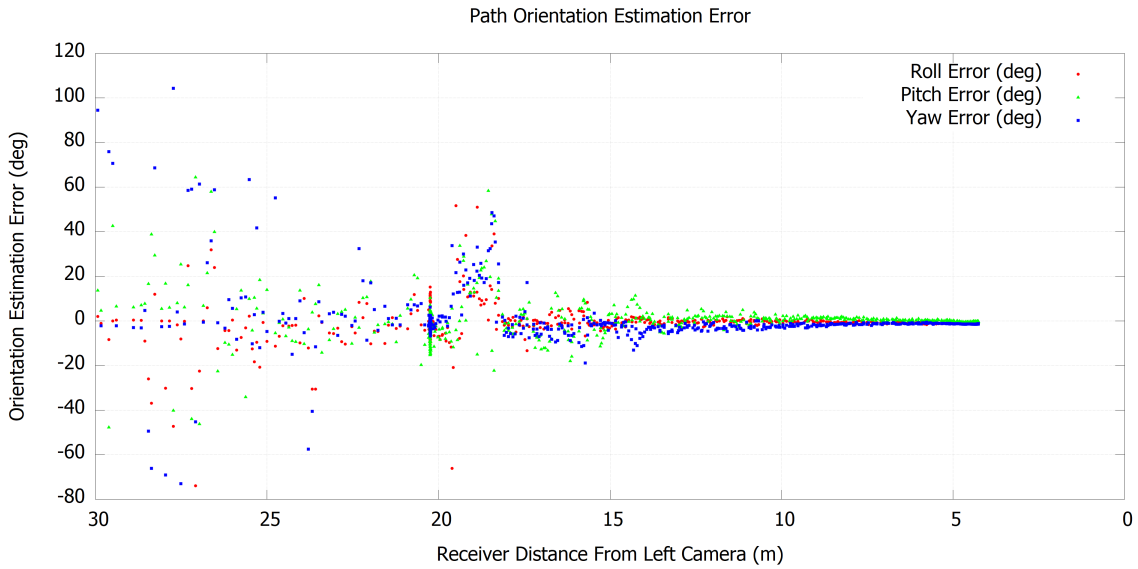

Figure 41. EO RPY Error for Test Run 2

www.manaraa.com

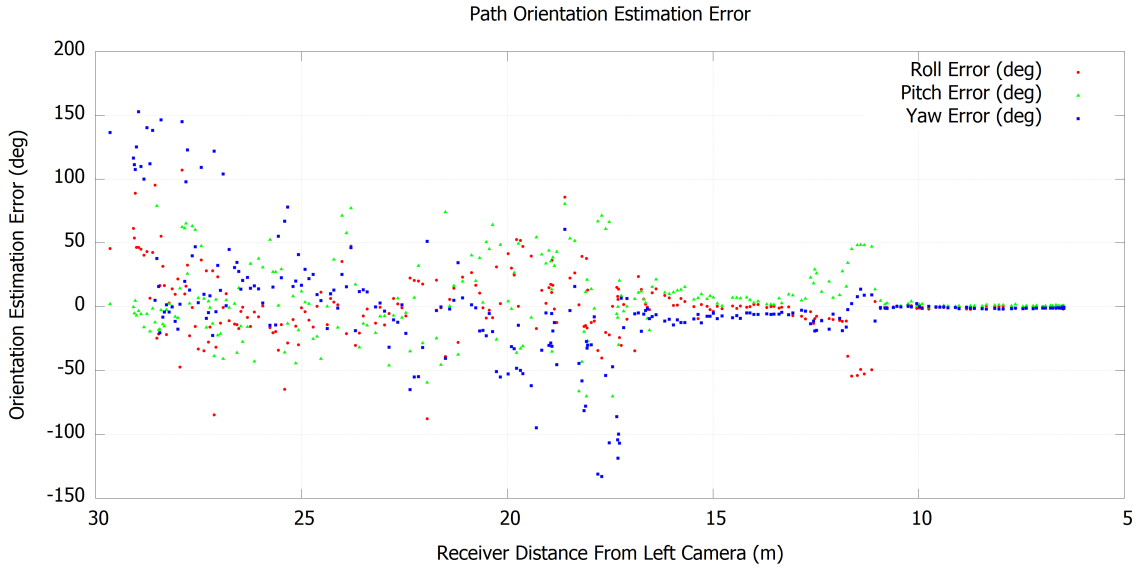

Figure 42. EO RPY Error for Test Run 3

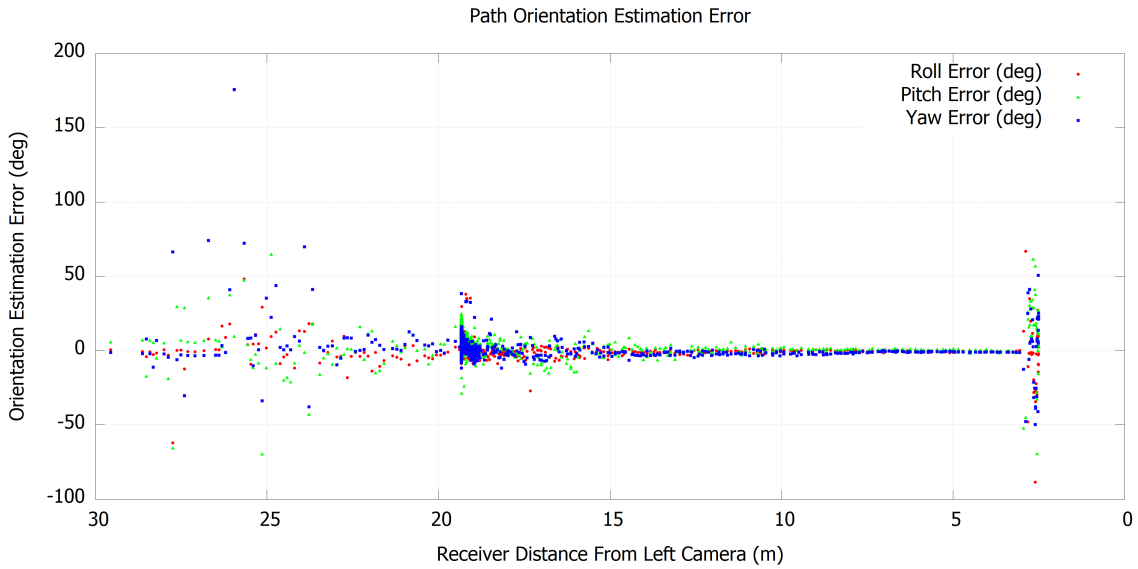

Figure 43. EO RPY Error for Test Run 4

www.manaraa.com

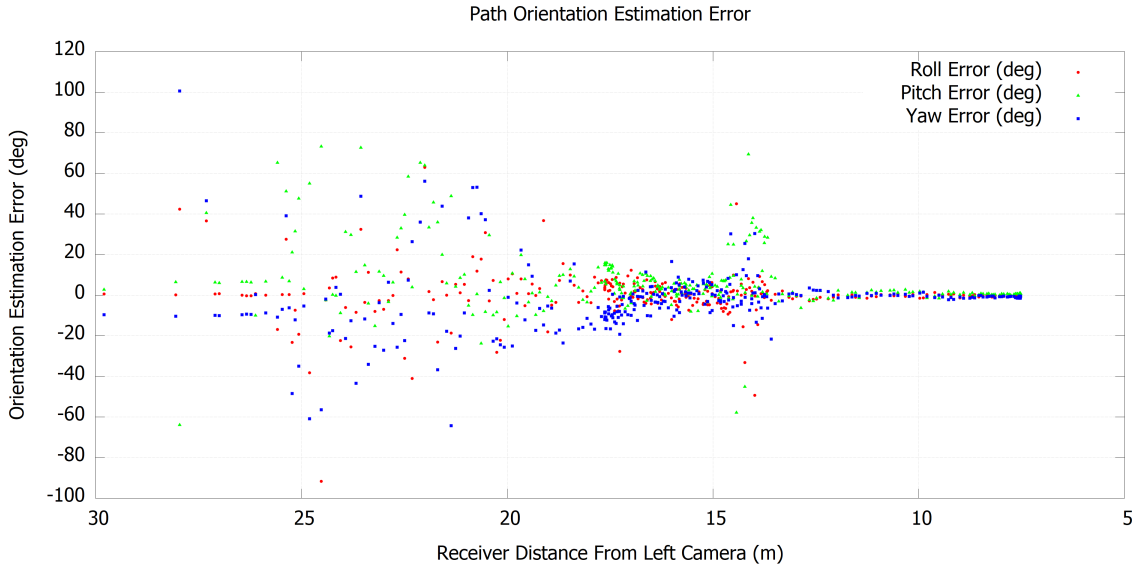

Figure 44. EO RPY Error for Test Run 5

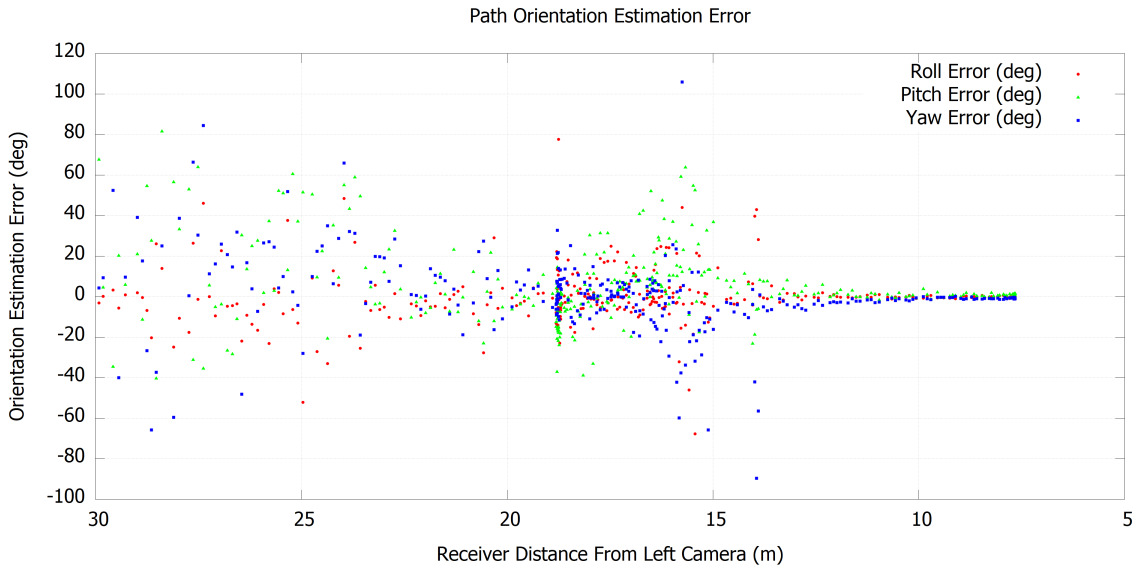

Figure 45. EO RPY Error for Test Run 6

www.manaraa.com

Figure 46. EO Position Error for Test Run 1

Figure 47. EO Position Error for Test Run 2

www.manaraa.com

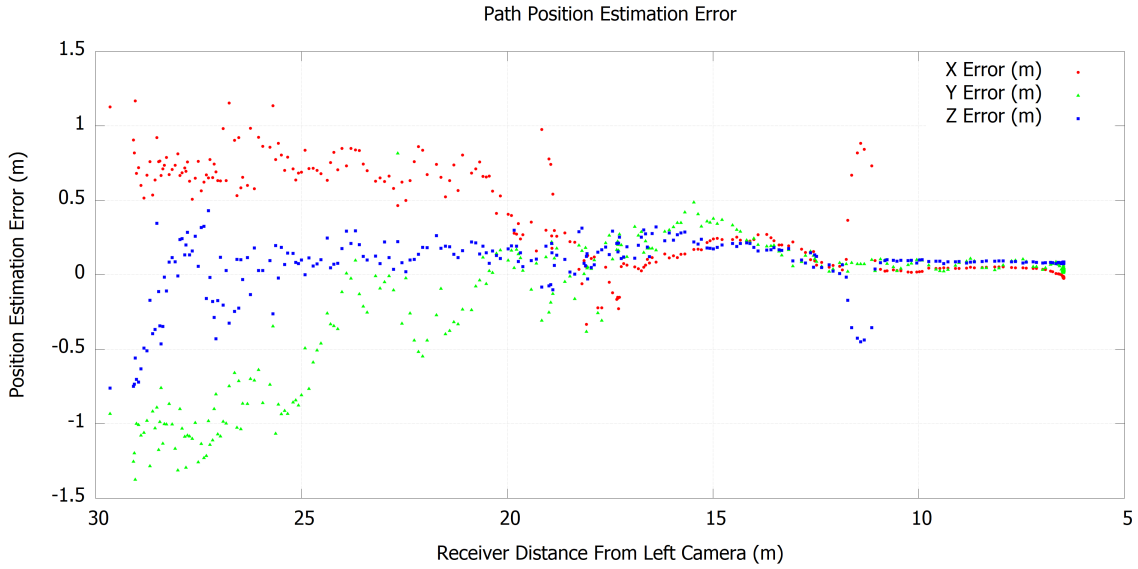

Figure 48. EO Position Error for Test Run 3

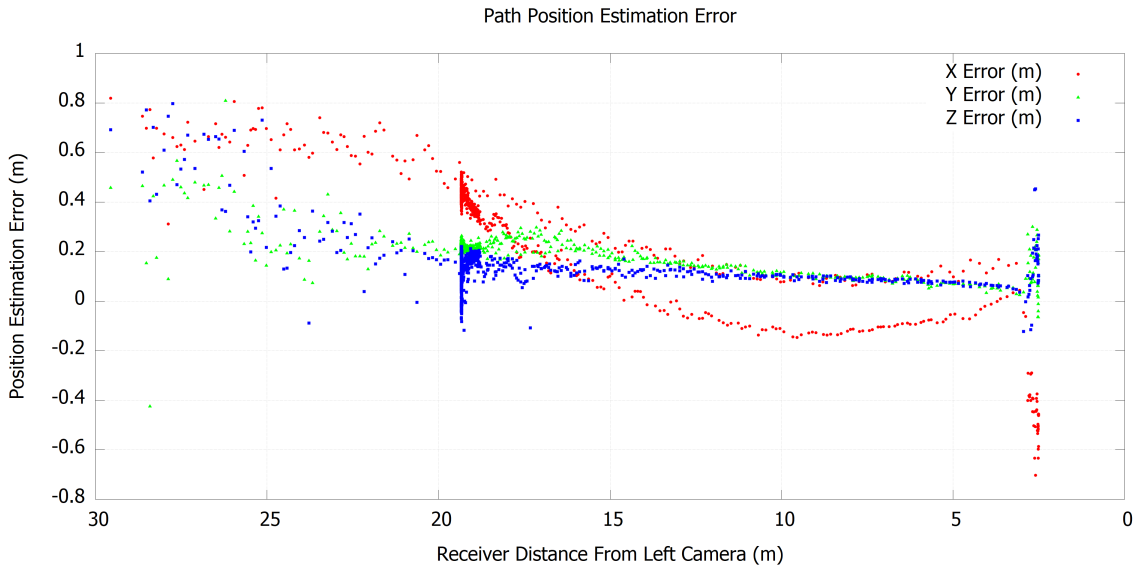

Figure 49. EO Position Error for Test Run 4

www.manaraa.com

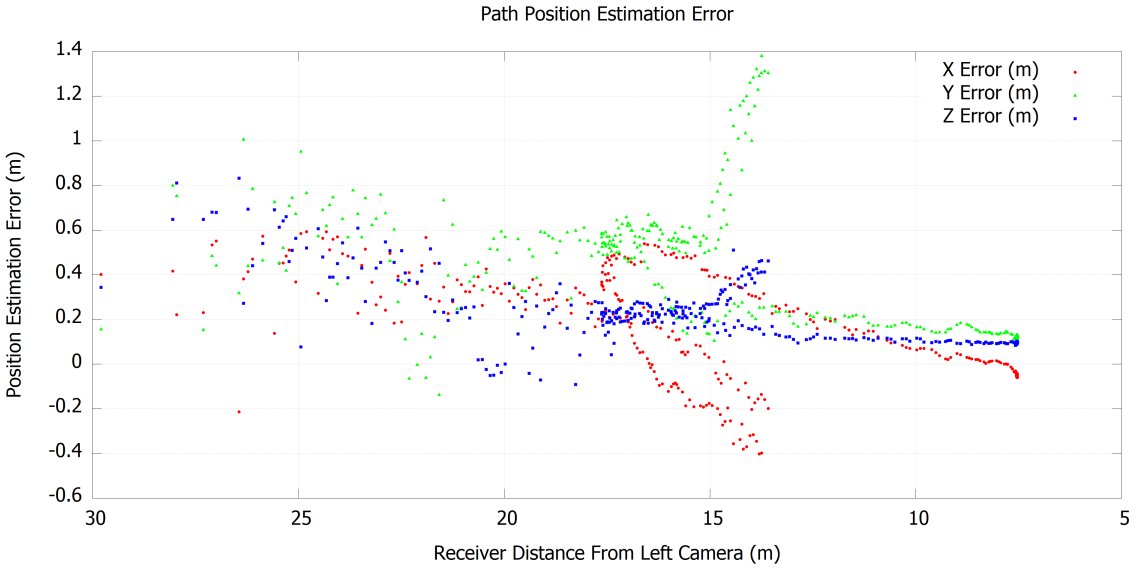

Figure 50. EO Position Error for Test Run 5

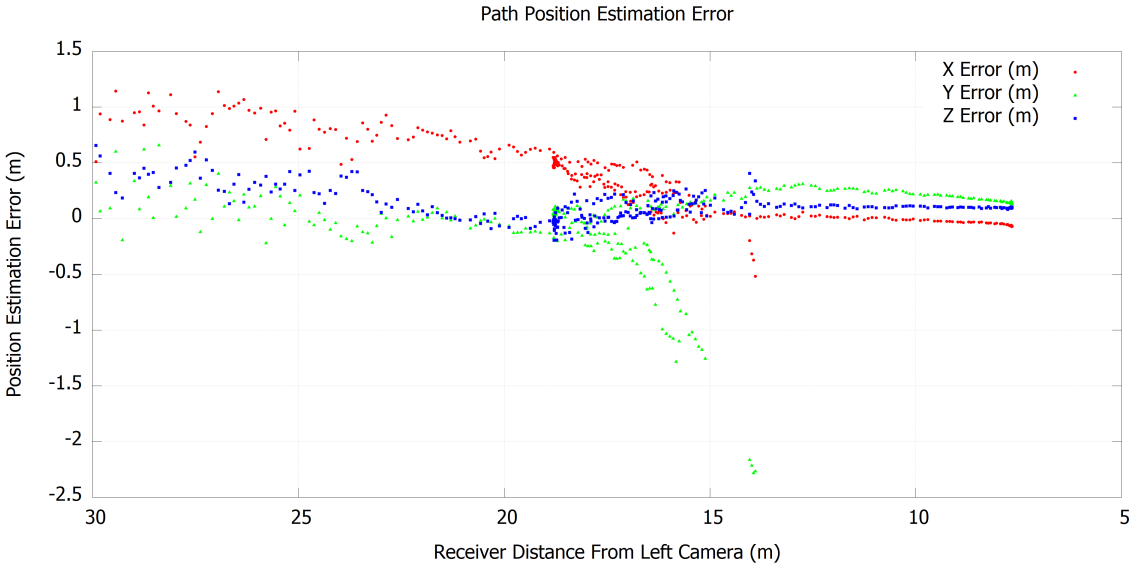

Figure 51. EO Position Error for Test Run 6

www.manaraa.com

4.4 Error Analysis

Calibration.

Using the IMU's reference frame for the position error, the depth error is relative to the x error. Although the depth error was typically around 10 centimeters or less, the error was the least linear component of the position error. This inconsistency is believed to be the result of imperfect calibration. Depth is the most difficult computation for stereo computer vision, so the calibration must be highly accurate to give good depth results. Calibration will attempt to calculate the most accurate intrinsic and extrinsic parameters, however, not all parameters will be perfectly calculated. Therefore, it may be necessary to fix some of the parameters to known values rather than relying on the calibration. In the case of the EO calibration, the focal length was adjusted to give better results. However, the IR calibration was not changed from its original output from MATLAB®.

The checkerboard used also made calibration difficult at times for the EO cameras because the metallic surface would reflect light and wash out some of the corners in the image. Due to the upward angle of the cameras, it also wasn't possible to capture calibration images with the checkerboard covering the entire image plane. Therefore, improving the initial calibration could increase the accuracy of the results. Additionally, adjusting the calibration parameters to more exact values for both the IR and EO cameras could also improve accuracy.

Timing Error.

Due to the data collection computer relying on its own clock's accuracy after syncing with GPS time, it's possible that the clock's drift from GPS time could affect the results. A drift in time would then misalign the images with the GPS truth data. If the approach rate during the experiments is assumed to be around 1.5 meters per

www.manaraa.com

second, and the clock has drifted by 1/30 of a second by the end of the experiment, then the resulting error would be a maximum of 5 centimeters. Since the clock drift would increase throughout the experiment, the error would be minor for most of the tests. However, the higher than usual position error in tests 5 and 6 could be from the clock drift, especially due to the consistency in the error between the IR and EO results. Therefore, regularly updating the CPU clock to GPS time would resolve the CPU drift error.

IMU Drift Error.

Each IMU can also have drift error if the IMU remains stationary. Since the pseudo tanker's IMU remained stationary during the test runs 1-6, the IMU accuracy would have drifted. However, the IMU drift would occur over time, which would eliminate fixing the drift with a constant offset. Therefore, moving the tanker between test runs could improve accuracy. For the actual flight tests with the C-12Cs, the IMUs will remain moving in-flight, so IMU drift error will not be an issue.

Physical Measurements.

All physical lever arm measurements were made using a tape measure. Since the lever arms required measuring the x, y, and z components, error could have occurred while adding each component together. Additionally, the measurements had to be "eyed up" using the tape measure, which also increased the possibility for error. Lever arms had to be measured between pseudo receiver IMU and GPS, between the pseudo tanker IMU and GPS, and between the pseudo tanker IMU and cameras, therefore, measurement error could be compounded from each of the separate measurements. Using an improved measuring system, such as laser measurements, could negate any measurement error.

www.manaraa.com

Summary of Results.

Given the many different components of the experiment and the various sources of error that had to be minimized, the relatively low position and orientation error achieved through stereo vision is good news for pose estimation and for AAR. Additionally, the consistent behavior between the IR and EO results proved useful for validating IR stereo vision as a legitimate source of pose estimation. Even without making any updates to the IR calibration, the IR results had a low amount of error. Additionally, the resolution of the IR cameras is lower than for the EO cameras, further proving the effectiveness of the IR cameras. The results also show that pose estimation can be completed in a real world environment with a high level of accuracy.

www.manaraa.com

V. Conclusion

Stereo vision provides a unique opportunity for solving the AAR problem due to the stereo cameras already equipped on next-generation tankers. And although there are many steps involved in the stereo computer vision process, all of these steps can be completed aboard a next-generation tanker. The ground experiments show that the camera technology and computer power is available to make accurate pose estimates. There is also room for the experiments to be improved and to reduce the error even further. In most cases, the pseudo approaches produced results with position error of less than 10 centimeters and RPY error typically around 2 degrees.

The accuracy of the pose estimates presented in the Results chapter is promising for the future of AAR. Both the IR and EO cameras showed similarly accurate results, providing variety in the stereo vision system that could be used for AAR. Although some research has been done with monocular and stereo EO systems, this research further validated the ability to create pose estimates using an EO stereo vision system. However, IR stereo vision is a new method for solving the AAR problem, and this research has shown that IR stereo vision can have the same accuracy as EO stereo vision. IR stereo vision may also be applicable to AAR scenarios that EO vision does not make possible, such as aerial refueling during the night. In addition to producing results with low error, the experiments conducted here have established a good framework for collecting valid and useful flight data during the upcoming flight tests.

5.1 Future Work

The Results chapter listed several potential sources of error. Each of these potential error sources should be further analyzed to either rule them out, or correct

www.manaraa.com

them to improve the stereo vision results. Improving the calibration process by using a better checkerboard for the EO cameras could easily improve the calibration process and potentially improve the intrinsic and extrinsic calibration parameters. Additionally, collecting calibration imagery with the cameras parallel to the ground would make it possible to cover the entire image plane with the checkerboard, thus improving camera calibration.

Increasing the variability of the experiments would further validate stereo vision for the various refueling scenarios that could occur. Experiments involving different receivers would prove useful, since a tanker will refuel different types of aircraft. Completing the experiments on various different days would help validate the system's durability over prolonged use, as will also be the case with a tanker. Lastly, the cameras should undergo additional environmental tests, such as temperature changes, light changes, and vibration changes.

To fully solve the AAR problem, flight test data must be analyzed. The upcoming flight tests provide an opportunity to collect and analyze real flight data. The data collected from the flight tests should be processed to determine pose estimates and validate stereo vision for aerial refueling. The results from the flight test data will lay the groundwork for stereo computer vision being used by tankers. Ultimately, these results could be what makes stereo computer vision a reality for AAR.

www.manaraa.com

Bibliography

1. Air Force Reserve Command. Aerial refueling. Accessed: https://www.afrc.af.mil/News/Photos/igphoto/2000575522/ on 7 February 2019.

2. Karen Roganov. F-35A instructor pilots qualify in aerial refueling. Accessed: https://www.af.mil/News/Article-Display/Article/109167/f-35a-instructor-pilots-qualify-in-aerial-refueling/ on 7 February 2019.

3. OpenCV. Camera Calibration and 3D Reconstruction. Accessed: https://docs.opencv.org/2.4/modules/calib3d/doc/camera_calibration_and_3d_reconstruction.html on 6 February 2019.

4. Yoram Yekutieli, Rea Mitelman, Binyamin Hochner, and Tamar Flash. Analyzing Octopus Movements Using Three-Dimensional Reconstruction. *Journal of Neurophysiology*, 98(3):1775–1790, 2007.

5. American Institute of Aeronautics and Aerospace. Aerial Refueling. Accessed: https://www.aiaa.org/microlesson37/ on 7 February 2019.

6. SC De Vries. UAVs and Control Delays. Technical report, TNO Defence Security and Safety Soesterberg (Netherlands), 2005.

7. Christopher A Parsons. Improving Automated Aerial Refueling Stereo Vision Pose Estimation Using a Shelled Reference Model. Master's thesis, Air Force Institute of Technology, 2017.

8. Richard Szeliski. *Computer Vision: Algorithms and Applications (Texts in Computer Science)*. Springer, 2011.

www.manaraa.com

9. Adrian Kaehler and Gary Bradski. *Learning OpenCV 3: Computer Vision in C++ with the OpenCV Library*. O'Reilly Media, 2016.

10. Richard Hartley and Andrew Zisserman. *Multiple View Geometry in computer vision*. Cambridge University Press, 2004.

11. Zhengyou Zhang. A Flexible New Technique for Camera Calibration. *IEEE Transactions on Pattern Analysis and Machine Intelligence*, 22(11):1330–1334, 2000.

12. Jace Robinson, Matt Piekenbrock, Lee Burchett, Scott Nykl, Brian Woolley, and Andrew Terzuoli. Parallelized Iterative Closest Point for Autonomous Aerial Refueling. In *International Symposium on Visual Computing*, pages 593–602. Springer, 2016.

13. Gary KL Tam, Zhi-Quan Cheng, Yu-Kun Lai, Frank C Langbein, Yonghuai Liu, David Marshall, Ralph R Martin, Xian-Fang Sun, and Paul L Rosin. Registration of 3D Point Clouds and Meshes: A Survey from Rigid to Nonrigid. *IEEE Transactions on Visualization and Computer Graphics*, 19(7):1199–1217, 2013.

14. Dmitry Chetverikov, Dmitry Svirko, Dmitry Stepanov, and Pavel Krsek. The Trimmed Iterative Closest Point Algorithm. In *Pattern Recognition, 2002. Proceedings. 16th International Conference on*, volume 3, pages 545–548. IEEE, 2002.

15. Peter R Thomas, Ujjar Bhandari, Steve Bullock, Thomas S Richardson, and Jonathan L Du Bois. Advances in Air to Air Refuelling. *Progress in Aerospace Sciences*, 71:14–35, 2014.

16. Ba Nguyen and Tong Lin. The Use of Flight Simulation and Flight Testing in the Automated Aerial Refueling Program. In *AIAA Modeling and Simulation Technologies Conference and Exhibit*, page 6007, 2005.

www.manaraa.com

17. Richard Burns, Curt Clark, and Ron Ewart. The Automated Aerial Refueling Simulation at the AVTAS Laboratory. In *AIAA Modeling and Simulation Technologies Conference and Exhibit*, page 6008, 2005.

18. Shuai An and Suozhong Yuan. Relative Position Control Design of Receiver UAV in Flying-Boom Aerial Refueling Phase. *ISA transactions*, 73:40–53, 2018.

19. Steven M Ross. Formation Flight Control for Aerial Refueling. Master's thesis, Air Force Institute of Technology, 2006.

20. Ryan P Dibley, Michael J Allen, and Nassib Nabaa. Autonomous Airborne Refueling Demonstration: Phase I Flight-Test Results. *AIAA Atmospheric Flight Mechanics Conference and Exhibit*, page 6639, 2007.

21. Walton R Williamson, Gregory J Glenn, Vu T Dang, Jason L Speyer, Stephen M Stecko, and John M Takacs. Sensor Fusion Applied to Autonomous Aerial Refueling. *Journal of Guidance, Control, and Dynamics*, 32(1):262–275, 2009.

22. Kevin Liu, Christopher Moore, Robert Buchler, Phil Bruner, Alex Fax, Jacob L Hinchman, Ba T Nguyen, David E Nelson, Fred Ventrone, and Brian R Thorward. Precision Relative Navigation Solution for Autonomous Operations in Close Proximity. In *Position, Location and Navigation Symposium, 2008 IEEE/ION*, pages 1246–1251. IEEE, 2008.

23. Daniel T Johnson, Scott L Nykl, and John F Raquet. Combining Stereo Vision and Inertial Navigation for Automated Aerial Refueling. *Journal of Guidance, Control, and Dynamics*, 2017.

24. Yunfeng Zhu, Yongrong Sun, Wei Zhao, Bin Huang, and Ling Wu. Relative Navigation for Autonomous Aerial Refueling Rendezvous Phase. *Optik*, 174:665–675, 2018.

www.manaraa.com

25. Chao-I Chen, Robert Koseluk, Chase Buchanan, Andrew Duerner, Brian Jeppesen, and Hunter Laux. Autonomous Aerial Refueling Ground Test Demonstration A Sensor-in-the-Loop, Non-Tracking Method. *Sensors*, 15(5):10948–10972, 2015.

26. II Curro and A Joseph. Automated Aerial Refueling Position Estimation Using a Scanning LiDAR. Master's thesis, Air Force Institute of Technology, 2012.

27. Yimin Deng, Ning Xian, and Haibin Duan. A Binocular Vision-Based Measuring System for UAVs Autonomous Aerial Refueling. In *Control and Automation (ICCA), 2016 12th IEEE International Conference on*, pages 221–226. IEEE, 2016.

28. Haibin Duan and Qifu Zhang. Visual Measurement in Simulation Environment for Vision-Based UAV Autonomous Aerial Refueling. *IEEE Transactions on Instrumentation and Measurement*, 64(9):2468–2480, 2015.

29. Mario L Fravolini, Marco Mammarella, Giampiero Campa, Marcello R Napolitano, and Mario Perhinschi. Machine Vision Algorithms for Autonomous Aerial Refueling for UAVs using the USAF Refueling Boom Method. In *Innovations in Defence Support Systems–1*, pages 95–138. Springer, 2010.

30. ML Fravolini, V Brunori, A Ficola, M La Cava, and G Campa. Feature Matching Algorithms for Machine Vision Based Autonomous Aerial Refueling. In *Control and Automation, 2006. MED'06. 14th Mediterranean Conference on*, pages 1–8. IEEE, 2006.

31. Mario L Fravolini, Giampiero Campa, and Marcello R Napolitano. Evaluation of Machine Vision Algorithms for Autonomous Aerial Refueling for Unmanned

www.manaraa.com

Aerial Vehicles. *Journal of Aerospace Computing, Information, and Communication*, 4(9):968–985, 2007.

32. Giampiero Campa, Marcello R Napolitano, and Mario L Fravolini. Simulation Environment for Machine Vision Based Aerial Refueling for UAVs. *IEEE Transactions on Aerospace and Electronic Systems*, 45(1):138–151, 2009.

33. Marco Mammarella, Giampiero Campa, Marcello R Napolitano, and Mario L Fravolini. Comparison of Point Matching Algorithms for the UAV Aerial Refueling Problem. *Machine Vision and Applications*, 21(3):241–251, 2010.

34. Lorenzo Pollini, Giampiero Campa, Fabrizio Giulietti, and Mario Innocenti. Virtual Simulation Set-Up for UAVs Aerial Refuelling. In *AIAA Modeling and Simulation Technologies Conference and Exhibit*, page 5682, 2003.

35. Long Xin, Delin Luo, and Han Li. A Monocular Visual Measurement System for UAV Probe-and-Drogue Autonomous Aerial Refueling. *International Journal of Intelligent Computing and Cybernetics*, 11(2):166–180, 2018.

36. John Valasek, Kiran Gunnam, Jennifer Kimmett, John L Junkins, Declan Hughes, and Monish D Tandale. Vision-Based Sensor and Navigation System for Autonomous Air Refueling. *Journal of Guidance, Control, and Dynamics*, 28(5):979–989, 2005.

37. Zachary C Paulson. Mitigating the Effects of Boom Occlusion on Automated Aerial Refueling Through Shadow Volumes. Master's thesis, Air Force Institute of Technology, 2018.

38. Nicholas J Seydel. Stereo Vision: A Comparison of Synthetic Imagery vs Real World Imagery for the Automated Aerial Refueling Problem. Master's thesis, Air Force Institute of Technology, 2018.

www.manaraa.com

39. Thomas R Stuart. Integrity Monitoring For Automated Aerial Refueling: A Stereo Vision Approach. Master's thesis, Air Force Institute of Technology, 2018.

40. Geodetics Inc. *Commercial User Manual*. 2649 Ariane Drive, San Diego, CA 92117.

41. Scott Nykl, Chad Mourning, Mitchell Leitch, David Chelberg, Teresa Franklin, and Chang Liu. An Overview of the STEAMiE Educational Game Engine. In *Frontiers in Education Conference, 2008. FIE 2008. 38th Annual*, pages F3B–21. IEEE, 2008.

42. Blender Online Community. *Blender - A 3D Modelling and Rendering Package*. Blender Foundation, Blender Institute, Amsterdam,

43. Joseph C Watts, Vernon L Diekmann, Raymond B Smith, Jon E Hannan, and William A Norton. Airworthiness and Flight Characteristics Evaluation, C-12A Aircraft. Technical report, Army Aviation Engineering Flight Activity Edwards AFB CA, 1976.

www.manaraa.com

REPORT DOCUMENTATION PAGE

Form Approved
OMB No. 0704–0188

The public reporting burden for this collection of information is estimated to average 1 hour per response, including the time for reviewing instructions, searching existing data sources, gathering and maintaining the data needed, and completing and reviewing the collection of information. Send comments regarding this burden estimate or any other aspect of this collection of information, including suggestions for reducing this burden to Department of Defense, Washington Headquarters Services, Directorate for Information Operations and Reports (0704–0188), 1215 Jefferson Davis Highway, Suite 1204, Arlington, VA 22202–4302. Respondents should be aware that notwithstanding any other provision of law, no person shall be subject to any penalty for failing to comply with a collection of information if it does not display a currently valid OMB control number. **PLEASE DO NOT RETURN YOUR FORM TO THE ABOVE ADDRESS.**

1. REPORT DATE *(DD–MM–YYYY)*	2. REPORT TYPE	3. DATES COVERED *(From — To)*
21-03-2019	Master's Thesis	May 2017 — Mar 2019

4. TITLE AND SUBTITLE

Infrared and Electro-Optical Stereo Vision for Automated Aerial Refueling

5a. CONTRACT NUMBER

5b. GRANT NUMBER

5c. PROGRAM ELEMENT NUMBER

6. AUTHOR(S)

Dallmann, William E., Capt, USAF

5d. PROJECT NUMBER

19G118

5e. TASK NUMBER

5f. WORK UNIT NUMBER

7. PERFORMING ORGANIZATION NAME(S) AND ADDRESS(ES)

Air Force Institute of Technology
Graduate School of Engineering and Management (AFIT/EN)
2950 Hobson Way
WPAFB OH 45433-7765

8. PERFORMING ORGANIZATION REPORT NUMBER

AFIT-ENG-MS-19-M-022

9. SPONSORING / MONITORING AGENCY NAME(S) AND ADDRESS(ES)

Ba T Nguyen
Aerospace Systems Directorate, Air Force Research Laboratory
2210 8TH ST
WPAFB OH 45433-7765
(937) 938-7765
Email: ba.nguyen@us.af.mil

10. SPONSOR/MONITOR'S ACRONYM(S)

AFRL/RQ

11. SPONSOR/MONITOR'S REPORT NUMBER(S)

12. DISTRIBUTION / AVAILABILITY STATEMENT

DISTRIBUTION STATEMENT A
APPROVED FOR PUBLIC RELEASE; DISTRIBUTION UNLIMITED.

13. SUPPLEMENTARY NOTES

This material is declared a work of the U.S. Government and is not subject to copyright protection in the United States.

14. ABSTRACT

Currently, Unmanned Aerial Vehicles are unsafe to refuel in-flight due to the communication latency between the UAVs ground operator and the UAV. Providing UAVs with an in-flight refueling capability would improve their functionality by extending their flight duration and increasing their flight payload. Our solution to this problem is Automated Aerial Refueling (AAR) using stereo vision from stereo electro-optical and infrared cameras on a refueling tanker. To simulate a refueling scenario, we use ground vehicles to simulate a pseudo tanker and psuedo receiver UAV. Imagery of the receiver is collected by the cameras on the tanker and processed by a stereo block matching algorithm to calculate a position and orientation estimate of the receiver. GPS and IMU truth data is then used to validate these results.

15. SUBJECT TERMS

Automated Aerial Refueling, Stereo Vision, Infrared, Electro-Optical, Computer Vision, Virtual World, Camera Calibration

16. SECURITY CLASSIFICATION OF:			17. LIMITATION OF ABSTRACT	18. NUMBER OF PAGES	19a. NAME OF RESPONSIBLE PERSON
a. REPORT	b. ABSTRACT	c. THIS PAGE			Dr. Scott L. Nykl, AFIT/ENG
U	U	U	UU	82	19b. TELEPHONE NUMBER *(include area code)* (937) 255-3636 x4395

www.manaraa.com